2008-04-22

Development of a Miniature VTOL Tail-Sitter Unmanned Aerial Vehicle

Jeffrey V. Hogge
Brigham Young University - Provo

DEVELOPMENT OF A MINIATURE VTOL TAIL-SITTER UNMANNED AERIAL VEHICLE

by

Jeffrey V. Hogge

A thesis submitted to the faculty of

Brigham Young University

in partial fulfillment of the requirements for the degree of

Master of Science

Department of Mechanical Engineering

Brigham Young University

August 2008

BRIGHAM YOUNG UNIVERSITY

GRADUATE COMMITTEE APPROVAL

of a thesis submitted by

Jeffrey V. Hogge

This thesis has been read by each member of the following graduate committee and by majority vote has been found to be satisfactory.

Date	W. Jerry Bowman, Chair
Date	Timothy W. McLain
Date	Scott L. Thomson

BRIGHAM YOUNG UNIVERSITY

As chair of the candidate's graduate committee, I have read the thesis of Jeffrey V. Hogge in its final form and have found that (1) its format, citations, and bibliographical style are consistent and acceptable and fulfill university and department style requirements; (2) its illustrative materials including figures, tables, and charts are in place; and (3) the final manuscript is satisfactory to the graduate committee and is ready for submission to the university library.

Date

W. Jerry Bowman
Chair, Graduate Committee

Accepted for the Department

Matthew R. Jones
Graduate Coordinator

Accepted for the College

Alan R. Parkinson
Dean, Ira A. Fulton College of
Engineering and Technology

ABSTRACT

DEVELOPMENT OF A MINIATURE VTOL TAIL-SITTER

UNMANNED AERIAL VEHICLE

Jeffrey V. Hogge

Department of Mechanical Engineering

Master of Science

The design, analysis, construction and flight testing of a miniature Vertical Take-Off and Landing (VTOL) tail-sitter Unmanned Aerial Vehicle (UAV) prototype is presented in detail. Classic aircraft design methods were combined with numerical analysis to estimate the aircraft performance and flight characteristics. The numerical analysis employed a propeller blade-element theory coupled with momentum equations to predict the influence of a propeller slipstream on the freestream flow field, then the aircraft was analyzed using 3-D vortex lifting-line theory to model finite wings immersed in the flow field. Four prototypes were designed, built, and tested and the evolution of these prototypes is presented. The final prototype design is discussed in detail. A method for sizing control surfaces for a tail-sitter was defined. The final prototype successfully demonstrated controllability both in horizontal flight and vertical flight. Significant contributions included the development of a control system that was effective in hover as well as descending vertical flight, and the development of a strong but light weight airframe. The aircraft had a payload weight fraction of 14.5% and a maximum dimension of one meter, making it the smallest tail-sitter UAV to carry a useful payload. This project is expected to provide a knowledge base for

the future design of small electric VTOL tail-sitter aircraft and to provide an airframe for future use in tail-sitter research.

ACKNOWLEDGMENTS

Thanks are in order first and foremost to my wife and family for their interest and encouragement. Also, I would like to thank my graduate advisor, Dr. Bowman, and the members of my graduate committee for sharing their knowledge and experience. Finally, I express my appreciation to all of the professors and staff members of the BYU Mechanical Engineering department who have helped me learn the basics of engineering and obtain a wonderful education.

Table of Contents

List of Tables

List of Figures

Nomenclature

α	Angle of attack
β	Wing geometric twist angle
δ	Induced drag factor
γ_{total}	Propulsion system efficiency
λ	Taper ratio
λ_{vt}	Vertical tail taper ratio
μ	Viscosity
ω	Propeller rotational velocity
ρ	Density
σ	Static margin
θ	Leading edge sweep angle
Λ	Propeller pitch
Π	Proportionality constant
A_{vane}	Control vane area
AR	Aspect ratio
AR_{vt}	Vertical tail aspect ratio
b	Wing span
$C_{battery}$	Battery Capacity
$C_{D,0}$	Parasite drag coefficient
C_D	Finite wing drag coefficient
$c_{l,max}$	Infinite wing maximum lift coefficient
$C_{L,max}$	Finite wing maximum lift coefficient
c_l	Infinite wing lift coefficient
C_L	Finite wing lift coefficient
C_m	Moment coefficient
c_{mac}	Mean aerodynamic chord
C_n	Z-axis moment coefficient
$c_{r,vt}$	Vertical tail root chord
c_r	Root chord
$c_{t,vt}$	Vertical tail tip chord
c_t	Tip Chord
C_T	Thrust coefficient
CG	Aircraft center of gravity

D	Propeller diameter
e	Oswald efficiency factor
f_{area}	Control vane area fraction
h_{vt}	Vertical tail height
J	Propeller advance ratio
K	Induced drag coefficient
l_{np}	Distance from CG to x_{np}
l_{vt}	Vertical tail moment arm
n_{vanes}	number of control vanes
P	Power
Re	Reynolds number
S	Planform area
S_{vt}	Vertical tail planform area
t	Flight time
T	Thrust
V	Airspeed
V_∞	Freestream velocity
$V_{battery}$	Battery Voltage
V_{stall}	Stall velocity
V_{vt}	Vertical tail volume fraction
W	Weight
$W_{battery}$	Battery weight
$W_{electronics}$	Electronics system weight
$W_{payload}$	Payload weight
$W_{propulsion}$	Propulsion system weight
x_{ac}	Wing aerodynamic center
x_{np}	Aircraft neutral point
$X_{structure}$	Structure weight fraction
y_{mac}	Span-wise offset of the mean aerodynamic chord

Chapter 1

Introduction

1.1 Background

Unmanned Aerial Vehicles (UAVs) are becoming more useful everyday because advancements in aerodynamics, propulsion, computers, and sensor technologies allow the aircraft to be used in increasingly diverse roles. As these roles become more diversified, aircraft need to continually adapt in order to perform multiple tasks efficiently with a single airframe. Aircraft are typically classified as conventional aircraft or rotor craft. Each of these classifications has advantages and disadvantages depending on the assigned mission. Conventional aircraft are capable of long flight times, ranges, and speeds that are not attainable in a rotor craft. However, rotor craft have the advantage of being able to hover and perform vertical takeoffs and landings without the need for runways, special launch and recovery equipment, or other infrastructure. They can also perform tasks such as perch-and-observe in the middle of a mission. The integration of the advantages of both vehicles into a single airframe provides the most effective design. The design, analysis, and construction of a VTOL UAV pose some difficult challenges. However, these challenges are not insurmountable and this project demonstrated that a VTOL UAV can be successfully developed.

Conventional aircraft are sometimes classified according to capability as follows:

- CTOL: Conventional Takeoff and Landing aircraft, which are the most common.
- VTOL: Vertical Takeoff and Landing aircraft that have the ability to takeoff and land vertically as well as hover.

- STOL: Short Takeoff and Landing aircraft, as the name states, use a shorter takeoff and landing run than a CTOL aircraft.

- STOVL: Short Takeoff and Vertical Landing aircraft cannot takeoff vertically at maximum weight, but do have enough power to be considered capable of short takeoffs. As weight is reduced due to fuel burn or expenditure of ordinance, the vehicle reaches a weight which allows hover and vertical landing.

- V/STOL: A different designation for STOVL aircraft that have a combination of short takeoff and vertical landing capabilities.

- VATOL: Vertical Attitude Takeoff and Landing aircraft are a subclass of VTOL aircraft which remain in a vertical attitude during takeoff, hover, and landing maneuvers. They are also known as tail-sitter aircraft.

VTOL aircraft development poses many difficult engineering challenges. Raymer [1] provides an excellent source of detailed information for these challenges. The most pertinent of the challenges include airframe configuration, balance of the aircraft, and propulsion selection. Each of these challenges will be addressed in the following paragraphs.

1.1.1 Airframe Configuration

The development of full scale VTOL aircraft began in the early 1950s and several airframe configurations have been explored through the years. McCormick [2] suggests several different classifications for these configurations of VTOL aircraft. These classes are vectored thrust, compound, tilt-wing, tilt-rotor, and tail-sitter aircraft. Figure 1.1 shows an example of each configuration.

Vectored Thrust

Vectored thrust is the most widely employed design used for VTOL aircraft. In this configuration, the thrust from the main engine can be vectored downward to provide a vertical lift force during takeoff and landing operations. Examples of this type of vehicle

include the Harrier Jump Jet and the new Lockheed Martin F-35 Lightning II. Typically, this design solution requires the employment of special mechanical devices to redirect the thrust and some sort of reaction control system (RCS) to control the vehicle while in hover. The aircraft remains in a horizontal position while thrust from the main engine is deflected downward to provide the lifting force. The RCS uses engine bleed-air ejected through nozzles in the nose, tail, and wingtips of the aircraft to provide stabilization and control.

Compound Aircraft

Compound aircraft are considered a helicopter-airplane hybrid. Vertical flight is accomplished using a powered rotor just like a helicopter. During forward flight, the rotor is stationary and traditional wing surfaces provide lift while a separate propulsion system such as a propeller or jet engine provides the required forward thrust. An example of this type of vehicle is the Heliplane that is under development by Groen Brothers Aviation.

Tilt-Wing

The tilt-wing design is composed of a conventional aircraft with engines mounted in the wings. For vertical flight, the entire wing is rotated to a vertical orientation so the thrust from the main engines is directed downward. In horizontal flight, the wing rotates to the usual horizontal position to provide lift with engine thrust in the horizontal direction. This design has not been pursued in recent years, but an early example is the Vertol 76.

Tilt-Rotor

Similar to the tilt-wing design, the tilt-rotor employs wing mounted engines that can swivel to direct thrust downward to provide a vertical lift force. The engines rotate to a horizontal position during normal flight operations and are the main source of propulsion. The difference between the tilt-wing and tilt-rotor designs is that the wing is stationary in the tilt-rotor example. A classic example of the tilt-rotor design is the Boeing V-22 Osprey.

Tail-Sitter

A tail-sitter design employs an aircraft configuration that appears fairly conventional. However, as the name implies, the aircraft is designed to takeoff and land vertically while sitting on its tail, which requires some modifications to the structure of the tail. The same engine is used for both vertical and horizontal flight. This design was used in several prototypes in the early 1950s. These include the Lockheed XFV-1, the Convair XFY-1, and the Ryan X-13 Vertijet. These aircraft were built and tested but never put into production.

1.1.2 Balance

Regardless of the airframe configuration, a VTOL aircraft must be balanced properly in order to achieve both vertical and horizontal flight. During vertical flight, the total thrust vector must pass through the center of gravity of the vehicle. This is typically the most challenging problem associated with VTOL airframe configurations because extra weight and complexity is added to the vehicle in order to produce thrust in the appropriate locations to allow the vehicle to balance. As seen in the previous section on airframe configurations, this problem has been addressed by moving the propulsion systems nearer to the center of gravity, adding additional engines, or vectoring the thrust of the main engines.

1.1.3 Thrust Matching

The major difficulty encountered in the propulsion system design is what Raymer [1] terms thrust matching. The thrust required for a vehicle to take off vertically must exceed the weight of the vehicle. Raymer suggests a minimum thrust-to-weight (T/W) ratio of 1.3 while Stoney [3] refers to a minimum value of 1.05 with a desirable value of 1.15. However, in forward cruising flight the thrust required is considerably less and depends on the cruise lift-to-drag (L/D) ratio of the vehicle. Typical L/D ratios are in the range of 5 to 20. This leads to two distinct problems. First, since the propulsion system in a VTOL aircraft must be more powerful than in a conventional aircraft, the system is larger and adds weight to the vehicle. Second, in cruising flight the large propulsion system will not operate at optimum levels and the extra weight reduces available payload capacity. There

(a) Vectored Thrust

(b) Tilt Rotor

(c) Tilt Wing

(d) Compound Aircraft

(e) Tail-Sitter

Figure 1.1: Existing Manned VTOL Aircraft Configurations: (a) Vectored Thrust (b) Tilt Rotor (c) Tilt Wing (d) Compound Aircraft (e) Tail-sitter

are three configurations for propulsion systems. The first configuration consists of separate lift and cruise engines with the lift engine used only in vertical flight and the cruise engine used only in horizontal flight. The second configuration consists of a lift engine that is used to augment the thrust of a lift+cruise engine which operates in both vertical and horizontal flight. The final configuration involves the use of a single engine which operates in both flight regimes.

1.1.4 Background Summary

Each of the airframe configurations discussed by McCormick [2] has multiple advantages and disadvantages. The vectored thrust designs lend themselves very well to military jets with a large thrust to weight ratio. However, there is an added level of mechanical complexity in changing the direction of the thrust and in balancing and controlling the vehicle in hover. The mechanisms employed to accomplish these tasks add a significant amount of weight to the aircraft. Compound aircraft can accomplish the mission of a helicopter and an airplane, but to date none have demonstrated the ability to do so with significant advantages over conventional helicopters or airplanes. Tilt-wing and tilt-rotor aircraft employ a high degree of mechanical complexity to accomplish their tasks, and therefore suffer a weight penalty as well. Tail-sitter aircraft need modifications to the tail structure to support some type of landing gear. This modification is straightforward in most cases and the weight penalty incurred is less than in other configurations. In addition, the tail-sitter does not employ a separate lift engine or need to augment thrust with a separate engine, so there is less additional weight added from the propulsion system. This makes the tail-sitter the best option in terms of being able to perform well both in vertical and horizontal flight. There are, however, several problems with the tail sitter. Newsome and Anglin [4] suggest two of the most prominent. First, the engine size necessary to produce sufficient thrust is very large. This causes a substantial decrease in the payload and range of the aircraft. Second, the attitude of the cockpit during vertical takeoff, landing, and hover maneuvers is very uncomfortable for pilots and makes landing and entry/exit from the cockpit very difficult. Designers are still working with the question of which design concept is the best for a manned VTOL aircraft.

Figure 1.2: Pogo Aircraft

Analogous to full-scale aircraft, the tail-sitter UAV design gives the advantages of vertical take-off and landing, hover, and perch-and-observe capabilities similar to a helicopter. Additionally, the ability of the aircraft to generate lift while in horizontal flight from conventional wings gives the vehicle added value by allowing for faster, more efficient forward flight, improved range, and longer loiter time than a conventional helicopter. The problems associated with the original tail-sitter concepts can be reduced in a UAV. The vehicles are smaller and propulsion technology has made great improvements since the 1950s, making propulsion less of an issue. Also, the pilot has been removed from the actual aircraft so the orientation of the vehicle cockpit becomes a non-issue. The advantages of a tail-sitter UAV make it the design configuration of choice due to the potential to fill the need for effective flight from a multipurpose UAV.

1.2 Previous Work

Several tail-sitter UAV designs have been implemented in recent years with some success. Table 1.1 shows the designs that have been created, along with the corresponding maximum size, weight, and propulsion method for each vehicle. In addition, the commercially available radio-control tail-sitter Pogo design from Hobby Lobby [5] was sold for a short time as a model aircraft. This vehicle is shown in Fig. 1.2 and was used as a test platform for developing an autonomous control system for tail-sitter aircraft by Knoebel [6]. Work continues on the tail-sitter aircraft at Supaero, the University of Arizona, and the MLB company.

Table 1.1: Existing Tail-sitter UAV Designs

Manufacturer	**Model**	**Size**	**Weight**	**Propulsion**
Arcturus UAV	Tracker	NA	NA	Twin electric motors
Boeing	Heliwing	5.2 m	544 kg	Single turbojet turning two propellers
University of Sidney	Twing	2.13 m	29.5 kg	Twin 100cc gas motors and propellers
Aurora	Goldeneye 50	1.37 m	8.2 kg	Gas powered ducted fan
Aerovironment	Skytote	2.44 m	113.4 kg	Gas coaxial counter rotating propellers
MLB Company	V-Bat	1.52 m	22.7 kg	Gas powered ducted propeller
SUPAERO	Vertigo	.65 m	1.6 kg	Electric coaxial counter-rotating propellers
University of Arizona	Mini Vertigo	.37 m	.4 kg	Electric coaxial counter-rotating propellers
Naval Postgraduate School	Archytas	4.27 m	45.4 kg	Gas-powered ducted propeller

1.3 Motivation

The development of a miniature tail-sitter UAV has the potential to fulfill the need for a multi-objective airframe in a field with growing demand. A miniature design could be used in a number of fields, including military and civilian markets, for many purposes. These include search and rescue, reconnaissance, border patrol, meteorological monitoring, wildfire tracking, etc. A small vehicle that can takeoff and land vertically, yet has the range of a conventional takeoff and landing vehicle, will be very useful because it negates the need for a runway or other infrastructure such as launch and recovery equipment. It also makes transport and maintenance of the vehicle much easier. These advantages provide the impetus to create a successful tail-sitter UAV.

1.4 Objectives

The objective of this project was to successfully design, build, and fly the smallest useful tail-sitter UAV to date. The minimum design requirements that had to be met to achieve this objective were:

- Maximum dimension of less than 1 meter
- Useful payload of 200 grams
- Vertical Takeoff and Landing capability
- Tail-sitter configuration

The anticipated difficulties in this project were producing a robust, light weight airframe and ensuring adequate control in vertical flight. The airframe had to be designed to allow integration of the aircraft components and the payload while being strong enough to survive the rigors of flight, in addition to providing the required aerodynamic lift. Also, the airframe weight had to be minimized to allow the vehicle to achieve vertical flight. The goals of a strong and light airframe were competing objectives. Control of the vehicle in vertical flight was also critical, especially in descending vertical flight where the free-stream velocity component is completely reversed in comparison with horizontal flight.

1.5 Contributions

Contributions from this project were fourfold. First and most significant, a successful miniature VTOL tail-sitter UAV was developed and flown which had a useful payload capacity of 200 grams. Second, a control system was developed which allowed the airplane to be completely controlled in vertical flight while flying both in and out of ground effect. Third, an airframe was developed which proved stable and controllable in horizontal flight. Last, the Aither analysis software proved to be a very useful tool for predicting the performance of small VTOL aircraft.

1.6 Summary

The driving influence for the development of VTOL UAVs is the creation of a single airframe that can operate effectively in both horizontal and vertical flight, allowing the completion of a myriad of missions. Previous work on full-scale and unmanned VTOL aircraft has shown some success and helped to identify some of the major challenges associated with VTOL flight. These include thrust matching, balance, and airframe configuration. There are many different airframe configurations available for VTOL aircraft, and the tail-sitter design was chosen for further development. The objective of the project was to successfully design, build, and fly the smallest useful tail-sitter UAV to date. The anticipated difficulties were airframe weight and adequate vertical flight control.

Chapter 2

Design Process

2.1 Introduction

This chapter describes the design process used to develop the airframe configuration of the tail-sitter UAV. The design process is explained in detail, then the concept generation and selection is defined.

2.2 The Design Process

The design process used throughout this project is shown in Fig. 2.1 and is based on the process defined by Ulrich and Eppinger [7]. The process began with the establishment of the key design requirements and specifications for the UAV. Next, multiple design concepts were proposed and then scored based on the established specifications. The concept which showed the most potential to fulfill the specifications was selected and designed in detail. Finally, flight testing was done to determine whether the prototype actually fulfilled the specifications. As the figure shows, this process allowed for changes not only to the design, but also to the design requirements if the prototype was unsuccessful.

2.3 Establish Design Specifications

The process of developing the tail-sitter UAV began with the specification of key design requirements and parameters. For this aircraft, the design requirements shown in Table 2.1 and the design parameters shown in Table 2.2 were chosen. These requirements and parameters quantify the objective stated in Chapter 1, which was to design, build, and fly the smallest useful tail-sitter UAV to date. To establish these specifications, the

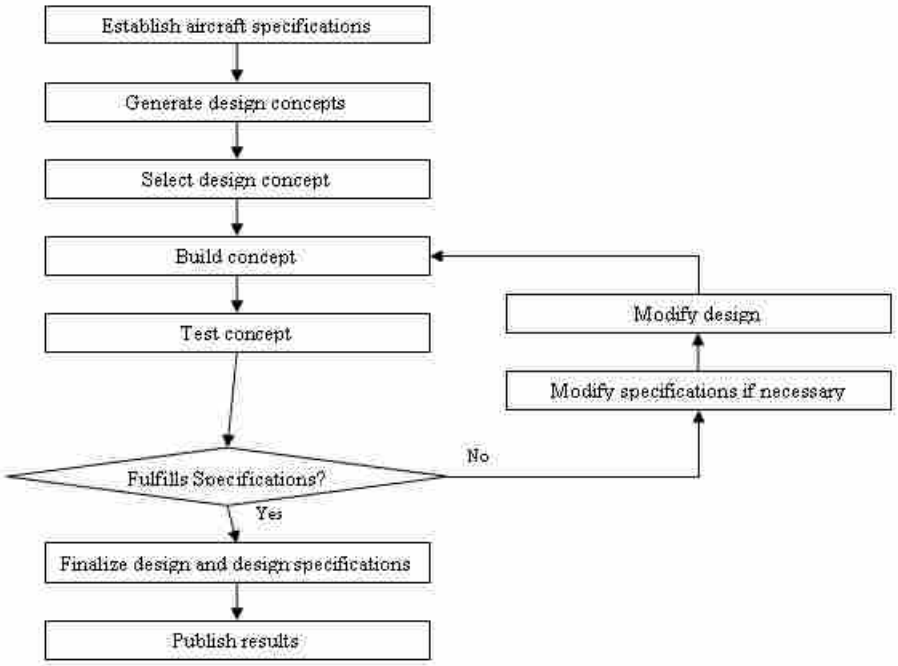

Figure 2.1: Design Process Flowchart

mission of the tail-sitter was considered and experience with the Pogo radio-control tail-sitter aircraft were taken into account. Specifically, the vehicle was designed to be able to takeoff vertically, transition to horizontal flight and perform a mission, then return and land vertically. Experience with the Pogo aircraft showed that a tail-sitter will tip over at times, so safety and robustness were very important. For this reason, the design requirements excluded the use of an exposed propeller which could be damaged, broken, or cause flying debris if the aircraft tipped over or crashed.

2.4 Concept Generation

The design process step of Concept Generation began with a detailed study of previous tail-sitter aircraft. Both full-scale manned aircraft and smaller UAVs were studied to develop a knowledge of previous projects. Table 1.1 provides a list of the tail-sitter UAV designs that have been developed previously. The existing tail-sitter designs and the de-

Table 2.1: Design Requirements

Safe	No exposed propeller
Stable	Able to be flown horizontally by an average RC pilot Able to be flown both horizontally and vertically by autopilot
Simple	Build time of less than 10 hours
Durable	Able to survive 5 hard landings without repair
Multi-purpose	Able to land vertically and conventionally

Table 2.2: Design Parameters

Useful payload	.20 kilograms
Hover endurance	10 minutes
Loiter endurance	30 minutes
Ground footprint	.14 meter ^{2}
Minimum Thrust-to-Weight ratio	1.3
Maximum Dimension	1 meter
Maximum Mass	1.50 kilograms
Cruise airspeed	15 m/s

sign requirements were used to develop six different concepts as possible design solutions. These concepts will be discussed in the following paragraphs.

Conventional Aircraft

The conventional aircraft configuration was a promising concept due to the proven record of performance in horizontal flight. This design placed the propulsion system at the nose of the aircraft, followed by the main wings and a slightly modified tail section. With a few design changes and structural upgrades to the empennage in order to provide VTOL capability and control in hover, this concept had potential to perform well as a tail-sitter. Aerovironment developed this concept into the Skytote, shown in Fig. 2.2.

Figure 2.2: Aerovironment Skytote

Canard Aircraft

The canard aircraft concept has also been used for full-scale and UAV type aircraft for many years. This design placed the horizontal stabilizer at the nose of the aircraft with the main lifting surface near the tail. The propulsion could be arranged as a conventional tractor, a pusher, or with multiple propulsion systems placed on the wings. Figure 2.3(a) shows the T-Wing tail-sitter developed at the University of Sidney, see [8]. Figure 2.3(b) shows the Aerohawk UAV developed by Sky Technology Vehicle Design and Development Company, see [9] for more details. Both of these canard designs demonstrated that this concept is viable for a tail-sitter aircraft.

Delta Wing Aircraft

The delta wing configuration also offered a promising tail-sitter concept due to robustness and ease of construction. The low aspect ratio wing is stronger compared to higher aspect ratios, and the propulsion could be arranged in a pusher or a tractor configuration.

(a) T-Wing (b) Aerohawk

Figure 2.3: Canard tail-sitter UAVs (a) T-Wing (b) Aerohawk

Figure 2.4 shows the design concept evaluated in this project. The Pogo aircraft is similar to this design.

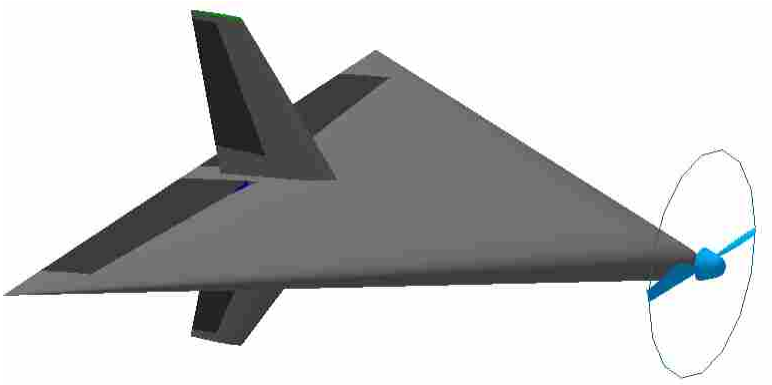

Figure 2.4: Delta Wing Tail-sitter Configuration

Flying Wing Aircraft

The flying wing aircraft had not been used previously in any tail-sitter applications, but it had the potential to do so. Similar to the delta wing concept, the flying wing was potentially quicker and easier to build because a fuselage is not required. However, the higher aspect ratio of the wing distinguishes the flying wing from the delta wing concept. This allows the aircraft to fly more efficiently which translates to longer flight times and greater range.

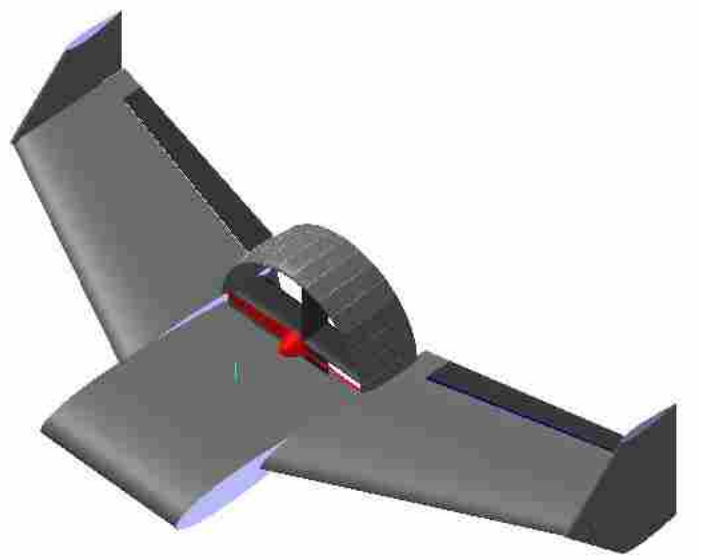

Figure 2.5: Flying Wing Tail-sitter Configuration

Biplane Canard Aircraft

The biplane canard offered a unique solution for a tail-sitter UAV. Structure exists for adding rudders between the upper and lower wing surfaces behind the propellers without adding any extra structural members. Efficiency is reduced due to aerodynamic interference between the wings. The design concept is shown in Fig. 2.6.

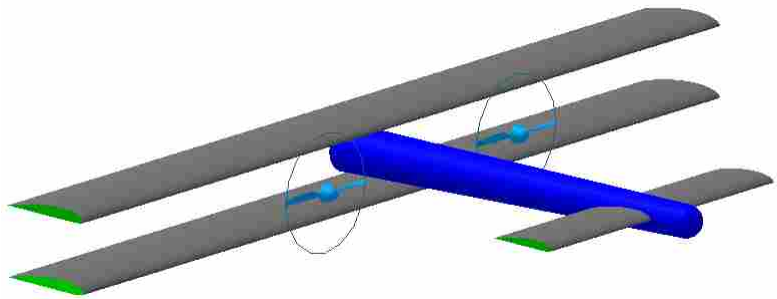

Figure 2.6: Biplane Canard Tail-sitter Configuration

H-Wing Aircraft

The H-wing aircraft concept is very unconventional but held promise for use as a tail-sitter, even with a low aspect ratio wing. With two propulsion systems arranged as shown in Fig. 2.7 with counter rotating propellers, the wing tip vortices are reduced by the propeller slipstreams. In addition, the propeller slipstream on the main wing reduces the effective angle of attack and could lead to better behavior during transition to and from horizontal flight from vertical flight. A similar concept, designated V-173, was developed into a full scale experimental aircraft by Vought during the early 1940's. That aricraft was considered a STOL vehicle because it did not have the ability to hover. The Arcturus Tracker seems to have been similar to this concept as well, but very little information is available on this model and it is doubtful that the vehicle made it past the prototype stage.

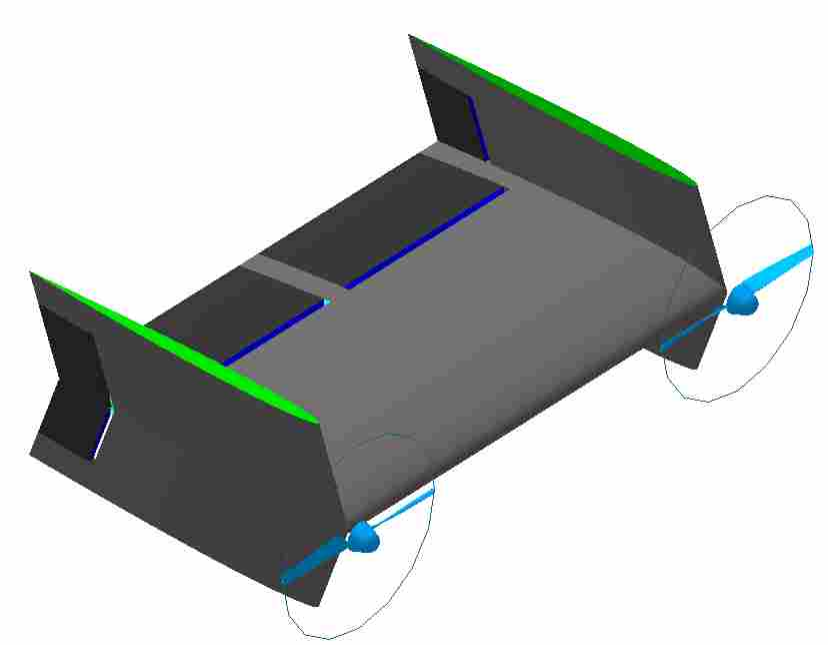

Figure 2.7: H-Wing Tail-sitter Configuration

2.5 Concept Selection

To choose the best concept for development, the scoring matrix shown in Table 2.3 was used. The key design specifications are listed in the left column of the matrix and each design concept is listed along the top row. A score of 1,2, or 3 was given to each concept for each design specification, with one being the worst score and three the best. The results of the scoring process are interesting, as there are several designs which received nearly the same score. However, the flying wing concept had the highest score and thus it was chosen for development into a tail-sitter UAV.

Table 2.3: Concept Selection Matrix

	Design Concept					
Design Specification	Conventional	Canard	Delta Wing	Flying Wing	Biplane Canard	H wing
Takeoff and land in a vertical attitude (tail-sitter)	1	2	3	2	3	3
Hover for 15 minutes	2	2	2	2	1	2
Loiter for 30 minutes	3	3	2	3	2	1
Carry a 200g useful payload	3	3	2	3	2	2
Be able to tip over without damage to the vehicle	1	2	3	2	3	3
Be able to land conventionally without damage	3	3	1	3	3	1
Be small	2	2	2	2	2	2
Be controllable in hover	2	2	2	2	2	2
Be controllable in forward flight	3	2	2	3	2	1
Be easily built	2	2	3	2	1	2
Be electrically powered	3	3	3	3	3	3
Total	25	26	25	27	24	22

Probability of Success	
Very Probable	3
Probable	2
Improbable	1

2.6 Summary

The complete design process for the project is outlined in Fig. 2.1 and explained in detail. Six tail-sitter concepts were discussed and scored using the scoring matrix in Table 2.3. The flying wing concept was shown to have the highest score and was chosen for detailed development.

Chapter 3

Preliminary Aircraft Design

3.1 Introduction

The preliminary design of the aircraft was done by following a classical procedure similar to the process given by Corke [10]. First, a preliminary weight estimate was made, followed by the main wing design and the stabilizer design. Next, a propulsion system was analyzed and selected, the control system was designed, and the materials for construction were chosen. Finally, a revised and more detailed weight estimate was made. This chapter describes each of these steps in detail.

3.2 Weight Estimate

The initial weight estimate for the aircraft was calculated without prior knowledge of the weight of the aircraft structure. This posed no problem, because an estimate for the weight of the airframe as a percentage of the total weight of the aircraft was assumed and the total weight was then calculated using Eq. 3.1, as proposed by Bowman and Snyder [11].

$$W = \frac{W_{battery} + W_{propulsion} + W_{electronics} + W_{payload}}{1 - X_{structure}} \tag{3.1}$$

Experience has shown that for flying wing aircraft a value of .40 to .50 is appropriate for the structure weight fraction $X_{structure}$, which is defined as the percentage of the total aircraft weight derived from the structure, as seen in Eq. 3.2. An estimate of the weight of the battery $W_{battery}$, propulsion system $W_{propulsion}$, and electronics $W_{electronics}$ was obtained

with a preliminary selection of components, which would be revised when the total weight estimate W was refined. The payload weight $W_{payload}$ was defined in the design parameters.

$$X_{structure} = \frac{W_{structure}}{W} \tag{3.2}$$

3.3 Main Wing Design

The design of the main wing began with the selection of an airfoil and the calculation of the finite wing maximum lift coefficient, $C_{L,max}$. The maximum lift coefficient for an airfoil or infinite wing $c_{l,max}$ can be obtained from wind tunnel data or estimated numerically. For this project, the XFOIL program created by Mark Drela [12] was used to estimate airfoil characteristics. Anderson [13] suggests that a preliminary estimate of $C_{L,max}$ can be obtained by averaging $c_{l,max}$ from the root and tip airfoils of a wing, then reducing the result by 10% to account for the wing being finite. Due to the low Reynolds numbers and aspect ratios involved with this small UAV design project, a reduction of 20% was used as shown in Eq. 3.3.

$$C_{L,max} = .8\frac{(c_{l,max})_{root} + (c_{l,max})_{tip}}{2} \tag{3.3}$$

Once $C_{L,max}$ was estimated, the wing loading (W/S) and the total required wing area (S) were calculated with Eqs. 3.4 and 3.5 by choosing the minimum flying velocity, V_{stall}. For a conventional aircraft, V_{stall} corresponds to the landing speed. For a VTOL aircraft, V_{stall} corresponds to the minimum forward flight speed.

$$\frac{W}{S} = \frac{1}{2}\rho V_{stall}^2 C_{L,max} \tag{3.4}$$

$$S = \frac{W}{\left(\frac{W}{S}\right)} \tag{3.5}$$

Next, the layout of the wing was completed by choosing the aspect ratio AR, the taper ratio λ, the leading edge wing sweep θ, and the geometric twist β. Eqs. 3.6 to 3.10 from Anderson [13] were used to calculate the total wing span b, the root chord c_r, the

tip chord c_t, the mean aerodynamic chord c_{mac}, and the span-wise offset y_{mac} of the mean aerodynamic chord from the root chord.

$$b = \sqrt{S \cdot AR} \tag{3.6}$$

$$c_r = \frac{2S}{(\lambda + 1)b} \tag{3.7}$$

$$c_t = \lambda c_r \tag{3.8}$$

$$c_{mac} = \frac{2}{3}\left(\frac{1 + \lambda + \lambda^2}{1 + \lambda}\right) \tag{3.9}$$

$$y_{mac} = \frac{b}{6}\left(\frac{1 + 2\lambda}{1 + \lambda}\right) \tag{3.10}$$

With these values, geometry was used to calculate the location of the aerodynamic center of the wing x_{ac} using Eq. 3.11.

$$x_{ac} = \frac{c_{mac}}{4} + y_{mac} \tan\theta \tag{3.11}$$

Finally, the wing configuration was used to create estimates of the aircraft drag polar as well as curves of thrust and power required versus airspeed. These curves are very useful during propulsion system design and propulsion system component selection. The drag polar was calculated using Eq. 3.12 where $C_{D,0}$ is the zero lift drag coefficient and KC_L^2 is the drag due to lift. The factor K can be estimated from lifting line theory or calculated from published data using the Oswald efficiency factor e, as shown in Eq. 3.13. Anderson [14] provides an excellent discussion on the details of the development of the induced drag coefficient δ, which is related to the Oswald efficiency factor through Eq. 3.14.

$$C_D = C_{D,0} + KC_L^2 \tag{3.12}$$

$$K = \frac{1}{\pi e A R} \tag{3.13}$$

$$e = \frac{1}{1+\delta} \tag{3.14}$$

The thrust and power required versus airspeed curves were generated in five steps. First, a specific velocity V was chosen. From this velocity, the corresponding lift coefficient was calculated using Eq. 3.15. Next, the drag coefficient C_D was calculated using Eq. 3.12. The ratio C_L/C_D, which is equivalent to the lift-to-drag ratio L/D, was used to determine the thrust required at the chosen velocity as shown in Eq. 3.16. Finally, Eq. 3.17 was used to calculate the power required for horizontal flight.

$$C_L = \frac{2W}{\rho V^2 S} \tag{3.15}$$

$$T = \frac{W}{\left(\frac{L}{D}\right)} \tag{3.16}$$

$$P = T \cdot V \tag{3.17}$$

3.4 Stabilizer Design

The stabilizer design for a flying wing is simplified due to the fact that the vehicle does not have a traditional empennage. Yaw stability is derived from vertical stabilizers or winglets attached to the wing tips. For the tail-sitter UAV, the winglets were modified to extend both above and below the wing tips to provide additional area in the ground footprint when the vehicle rests in a vertical attitude on the ground. Preliminary sizing of the winglets was achieved by assuming that a single vertical stabilizer would be placed on the centerline of the aircraft and at a position which aligns it with the wing tips, as shown by the red vertical fin in Fig. 3.1. Anderson [13] suggests that Eq. 3.18 can be used to estimate the necessary size of this vertical tail fin, where S_{vt} refers to the area of the vertical

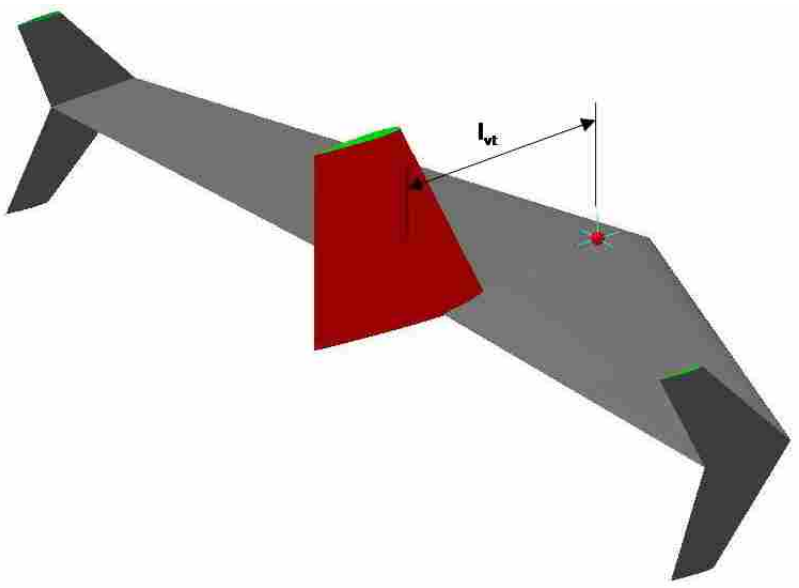

Figure 3.1: Vertical Winglet Sizing

tail and V_{vt} refers to the vertical tail volume fraction. A reference value of .04 is given for V_{vt} for a single vertical tail. Since two winglets were used, this value was divided in half. The linear distance from the center of gravity of the aircraft to the aerodynamic center of the single vertical fin is the moment arm l_{vt} in Eq. 3.18 and this distance is illustrated in Fig. 3.1.

$$S_{vt} = \frac{V_{vt} b S}{l_{vt}} \tag{3.18}$$

Once the necessary stabilizer area was determined, it was divided in half and two winglets of equal dimension were configured using the following equations to define the height h_{vt}, root chord $c_{r,vt}$, and tip chord $c_{t,vt}$, after selecting an appropriate aspect ratio AR_{vt} and taper ratio λ_{vt}.

$$h_{vt} = \sqrt{AR_{vt} \cdot S_{vt}} \tag{3.19}$$

$$c_{r,vt} = \frac{2S_{vt}}{(\lambda_{vt}+1)h_{vt}} \tag{3.20}$$

$$c_{t,vt} = \lambda_{vt} c_{r,vt} \tag{3.21}$$

Anderson [13] suggests an aspect ratio in the range of 1.3 to 3 for a vertical tail.

3.5 Propulsion System Selection

The propulsion system of a VTOL aircraft has increased performance requirements and design considerations over a CTOL vehicle. The major hurdle to overcome with VTOL propulsion is the design of a system that will provide static thrust greater than the weight of the vehicle. This must be accomplished while considering total flight endurance of the vehicle, the propulsion system weight allotment, and the vehicle control in hovering flight.

The most important factor that influences the performance of a VTOL aircraft is the thrust-to-weight ratio. To better understand the factors that affect the thrust, it is helpful to study the governing principles for a propeller propulsion system. The goal of an effective VTOL propulsion system is to maximize thrust while minimizing the power required to produce that thrust. The thrust produced by a propeller driven propulsion system is a function of the propeller diameter D, pitch Λ, and rotational speed ω, as well as the fluid properties of viscosity μ and density ρ and the free-stream fluid velocity V_∞. A dimensional analysis shows that there are three non-dimensional parameters which can be used to describe thrust. These are the pitch-to-diameter ratio Λ/D, the Reynolds number based on propeller diameter Re_D, and the advance ratio J. The dimensional analysis also shows that the thrust produced is proportional to the square of the rotational speed of the propeller and the diameter of the propeller raised to the fourth power. These relationships are shown in Eq. 3.22 through Eq. 3.25.

$$\frac{\Lambda}{D} \tag{3.22}$$

$$Re = \frac{\rho V_\infty D}{\mu} \tag{3.23}$$

$$J = \frac{2\pi V_\infty}{D\omega} \tag{3.24}$$

$$T = \rho\omega^2 D^4 \Pi \tag{3.25}$$

Phillips [15] proposes that the proportionality constant Π in Eq. 3.25 is

$$\Pi = \frac{C_T}{(2\pi)^2}$$

using the thrust coefficient C_T and writes the thrust equation as shown in Eq. 3.26.

$$T = \rho \left(\frac{\omega}{2\pi}\right)^2 D^4 C_T \tag{3.26}$$

The thrust coefficient C_T is a function of the pitch-to-diameter ratio, the Reynolds number, and the advance ratio defined previously. Examining Eq. 3.26 reveals that thrust is highly dependent on the propeller diameter and the rotational speed, which intuitively makes sense. However, the implications for a VTOL aircraft are very important. Essentially, this relation shows that the larger the diameter of the propeller, the better the thrust-to-weight ratio will be for the aircraft.

The classic momentum analysis of a propeller disk provides essential insight into the power required by a propeller propulsion system. Figure 3.2 shows a stream tube control volume placed around an ideal propeller.

Using a similar setup for a momentum analysis, Seddon and Newman [16] and McCormick [2] show that the power P required to produce a specific level of thrust is proportional to that thust and the propeller diameter as shown in Eq. 3.27.

$$P = \left[\frac{2T^3}{\rho\pi D^2}\right]^{1/2} \tag{3.27}$$

This relationship shows two very important details of the propulsion system. First, the power required to hover a VTOL aircraft is proportional to the weight of the vehicle raised to the 3/2 power. Thus, as has been stated, the weight must be kept to a minimum to reduce the power required to hover the aircraft. Second, the power required to hover is

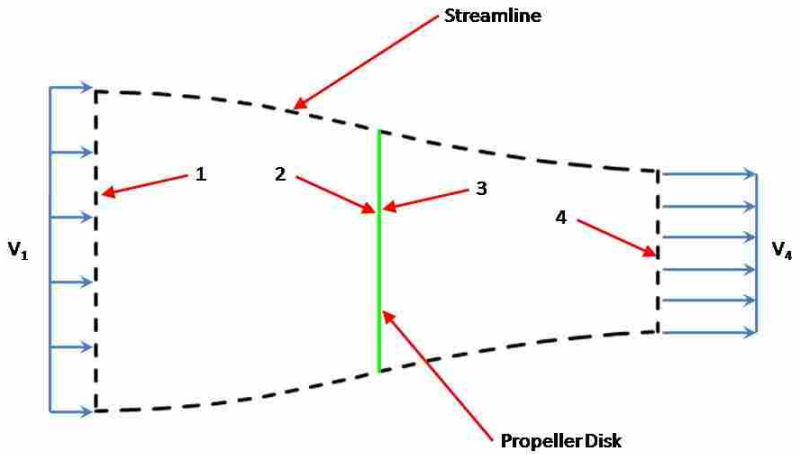

Figure 3.2: Stream Tube Control Volume

inversely proportional to the diameter of the propeller. This means that a large diameter propeller will require less power to produce the same amount of thrust as a propeller with a smaller diameter. Studying the thrust and power required in vertical flight led to the choice of a large diameter propeller.

The battery capacity required to complete the desired flight time was calculated using the estimate for power required at cruise velocity P and an estimate of the total propulsion system efficiency γ_{total}. The total power input to the propulsion system was determined by dividing the output power by the system efficiency. Equation 3.28 shows how this input power, multiplied by the desired flight time t and divided by the average battery voltage $V_{battery}$, resulted in the required battery capacity.

$$C_{battery} = \frac{Pt}{\gamma_{total} V_{battery}} \tag{3.28}$$

3.6 Control System Design

The propulsion system of a VTOL aircraft must be designed not only to allow the vehicle to hover but also to ensure that it can be maneuvered in all three dimensions while in vertical flight. This can be accomplished in a number of ways. For ease of construction and operation, a simple solution was to place control vanes directly aft of the propeller inside a protective shroud. Four vanes were placed in the duct in the shape of a plus-sign. These vanes allow the propeller slipstream to be deflected in order to actuate control of the vehicle in all three axes while it is hovering. The initial design used the two horizontal vanes as elevons, to actuate control in roll and pitch. These vanes were allowed to move differentially. The two vertical vanes were coupled to a single actuator and functioned only as a rudder to provide control in yaw. The location of the propeller and the control vanes is not arbitrary and has a significant effect on the performance of the vehicle. Experience has shown that placing the control vanes at a distance from the propeller, as with the Pogo [5] design, is a poor design choice. In descending vertical flight the propeller slipstream velocity is reduced as the distance from the propeller disk increases. This leads to ineffectual control in descending flight. In addition, when the vehicle is flying in ground effect, the propeller slipstream is deflected by the ground itself. If the control vanes are placed such that the deflection of the slipstream by the ground has more effect then the deflection of the control vanes, the vehicle will not be able to adequately maneuver. To overcome these two obstacles, the control system was configured with the four control vanes directly aft of the propeller inside the shroud. The shroud was located so as to maintain clearance from the ground when the vehicle is landed in order to ensure that the control vane effectiveness will not be mitigated by ground effect. Figure 3.3 represents graphically the influence of vane placement on control authority in the presence of ground effect. The upper control vane placement shown in the figure will be effective even when the vehicle is in ground effect. However, the lower control vane placement will not be effective due to the deflection of the air stream by the ground.

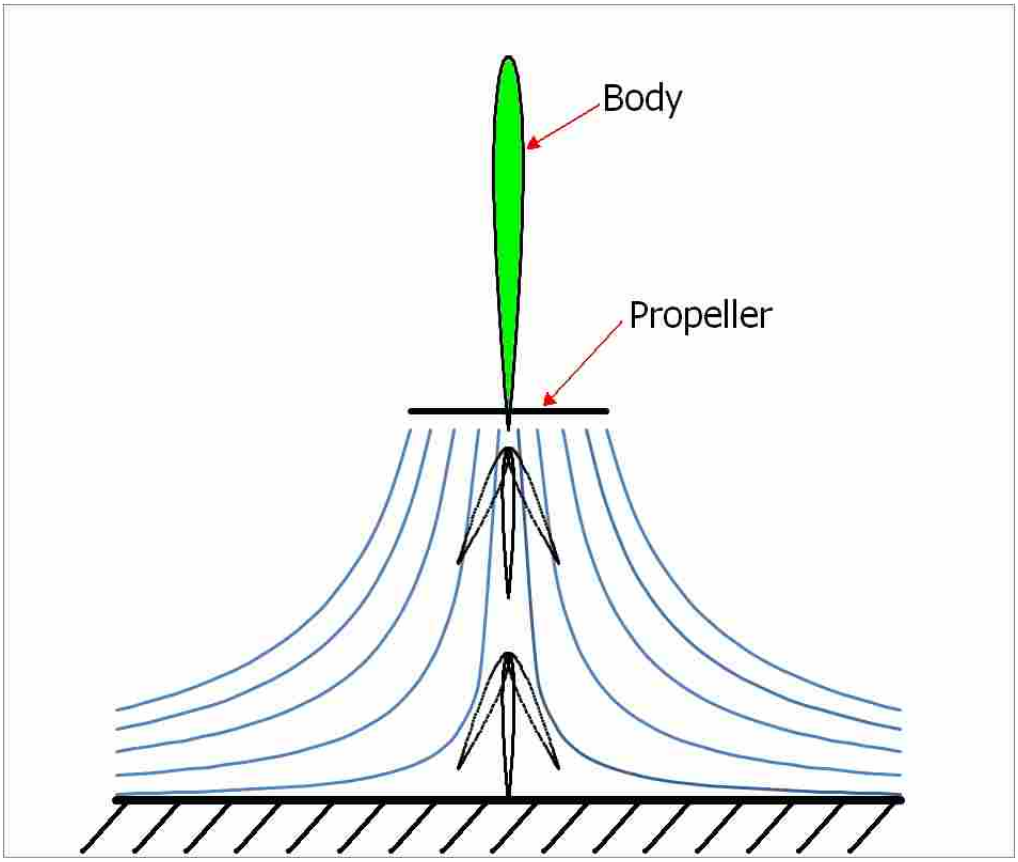

Figure 3.3: Control Vanes In and Out of Ground Effect

3.7 Material Selection

The materials selected to build the airframe of the tail-sitter UAV were very important to meeting the design weight allotment and in fulfilling the design requirement of being able to build the aircraft in less than 10 hours. In addition, the airframe had to be strong enough to survive at least five hard landings without repair in order to fulfill the durability requirement. Experience has shown that airframes made with an Extruded polypropylene (EPP) foam core are very durable and the foam can be shaped quickly with a hot wire cutter. For these reasons, EPP was chosen as the core material for the aircraft structure. It is common to use composite material such as fiberglass, carbon fiber, or kevlar as a covering material for UAVs. However, it is difficult to achieve an adequate bond to the EPP foam using these materials, and the resulting hard shell surrounding the flexible foam core is susceptible to damage in hard landings and crashes with additional separation of the cov-

ering from the foam core. In addition, the use of these materials requires much more time and equipment, so it was decided to avoid the use of these materials as much as possible. Instead of using composites, a simple method of covering the foam core with commercially available bi-directional fiber tape was used. This method has proven effective in providing the necessary structural reinforcement that a small UAV requires, as well as being simple to apply and very easy to repair in the event of damage to the vehicle.

3.8 Refined Weight Estimate and Balance

The preliminary weight estimate was made with an assumed value for the structure weight, and no effort was made initially to organize the airframe structure or components to balance the aircraft properly. As weight is a major factor for a VTOL aircraft, a more accurate estimate of weight is needed along with a method of laying out the aircraft to ensure proper balance. With initial sizing completed, the actual electronic components, motor, and battery to be used can be weighed and a center of mass determined for each. The remaining variables are the weight and center of mass of the airframe structure. Determining the center of mass of a wing section is not straightforward due to the irregular shape of the airfoil cross-section. A small algorithm was developed to calculate a reliable estimate of the weight and center of mass of linearly tapered swept wings. The source code is found in Appendix A. The program operated in the following manner:

1. Necessary input data was read into the program. This included the geometry of the wing as well as the root and tip airfoils. Since the wing was to be constructed so that it was solid rather than hollow, a density was input as well.

2. The area and centroid of the root airfoil were calculated by forming alternating triangles. First, two consecutive points were selected on the upper surface of the airfoil and one point was selected from the lower surface to form a triangle, as shown by the green triangle in Fig. 3.4. The resulting area and centroid of the triangle were calculated. The points were then alternated to form a new triangle consisting of two consecutive points on the lower surface and one on the upper surface as shown by the blue triangle in the figure. The points were again alternated and the process was

repeated to find the areas and centroids of all of the triangles contained in the airfoil. The areas of the triangles were summed and an area weighted average of the centroids of the trianges was calculated and divided by the total area to yield the airfoil centroid. This method ensured accurate results regardless of whether an airfoil had a concave or a convex profile.

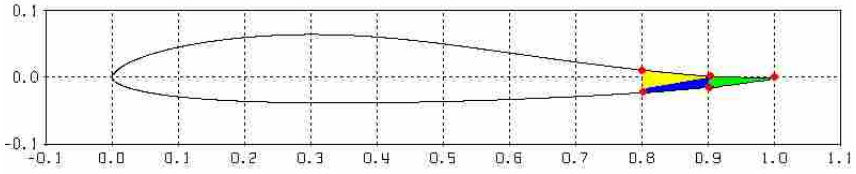

Figure 3.4: Alternating Triangles

3. The area and centroid of the tip airfoil were calculated if that airfoil was different from the root airfoil.

4. The wing volume and center of mass were calculated by dividing the wing section into a number of small elements which were assumed to have a rectangular planform. The volume and center of mass of these segments was easily calculated because a constant chord with no sweep was assumed for each element. The center of mass was located at the centroid of the airfoil and halfway across the segment span. The volume was simply the product of the airfoil area and the segment span. By summing the volumes and taking a volume weighted sum of the centers of mass, the total volume and center of mass were determined.

5. If a density was specified, the total mass and thus the weight were calculated.

Additional weight estimates needed to be made to account for the material used to cover the wings. This was calculated by determing the weight per unit area of the covering material. This value was then multiplied by twice the planform area, to account for the top and bottom surfaces, and an accurate estimate of the weight added due to the covering material was obtained.

Once the total weight and center of mass of the airframe structure were accurately estimated, the aircraft configuration was checked to ensure that placement of the components would ensure proper balance. This was a matter of using a mass weighted average to calculate the aircraft's center of mass and moving components as appropriate to ensure the center of mass coincided with the desired location.

3.9 Summary

The preliminary design steps explained in detail in the preceding sections were used to determine an initial configuration for the aircraft planform and the winglets. The propulsion system design steps showed that a large diameter propeller was preferrable to a smaller propeller for improving both thrust and power. In addition, the necessary battery size calculations were developed to allow selection of a battery pack. The control system for the aircraft was chosen to be a shroud aft of the propeller with four control vanes placed inside the shroud. Also, the influence of ground effect and propeller slipstream were very important in the control system design. EPP foam cores were selected as a core material for the aircraft structure with a covering made from bi-directional fiber tape. A refined weight estimate was made to improve the initial estimate as well as to evaluate the balance of the vehicle.

Chapter 4

Aircraft Analysis

4.1 Introduction

This chapter describes the software used to analyze the tail-sitter UAV designed using the methods in the previous chapter and discusses the results that are obtained from the analysis. Also, static stability of aircraft is discussed and the stability derivatives from the analysis program are used to estimate the stability of the tail-sitter UAV.

4.2 Aither

Aither was the software used for the analysis of the tail-sitter UAV. It is a combined wing and propeller numerical model for predicting the flight characteristics of small electric aircraft. In the program, blade element theory was combined with momentum conservation equations to determine the slipstream effects of propellers on the freestream velocity. Lifting line theory was used to analyze wings when they were immersed in the modified velocity field obtained from the combination of the freestream velocity and the propeller slipstream. Detailed documentation of the development of Aither is available in the thesis of Doug Hunsaker [17]. This program is well suited to the design of tail-sitter aircraft because the primary source of airflow around the aircraft during vertical flight is the propeller slipstream. The use of Aither in this project is described in the following sections.

4.2.1 Propellers

Propellers in an Aither aircraft model are defined using geometry, root and tip airfoils, and motor/battery combinations. The geometry of the propeller includes the diameter,

pitch, number of blades, root and tip chords, and the propeller hub diameter. Specific details about the root and tip airfoils used on the propeller are supplied in one of two ways. In the first and most accurate method, airfoil lift, drag, and moment coefficients from experimental data or other sources are supplied to Aither in the form of an input data file. Table 4.1 shows an example of the necessary input data. If no specific airfoil details are available, estimates for the lift slope, stall angle of attack, stalled lift slope, zero lift angle of attack, moment slope, and the zero lift moment coefficient are used to estimate airfoil performance.

Table 4.1: Aither Airfoil Input

Alpha(deg)	Cl	Cd	Cm
0	0	0	0
1	0.107985	0.000687	-0.00025
2	0.215688	0.002079	-0.00051
3	0.323015	0.004203	-0.00079
4	0.429847	0.007093	-0.00107
5	0.536033	0.0108	-0.00138
⋮	⋮	⋮	⋮
85	0.218591	1.9732	-0.47942
86	0.180488	1.97611	-0.48487
87	0.142197	1.97843	-0.49021
88	0.103763	1.98014	-0.49543
89	0.065232	1.98125	-0.50054

To obtain even more detailed results, information about the motor and battery combination used with the propeller need to be supplied as input. The motor needs to have the RPM/Volt, the no-load current, the armature resistance, and the mass specified. These specifications are commonly supplied by the motor manufacturer. The battery needs the capacity, voltage, impedance, mass, discharge rate, number of cells and battery composition to be specified. The electronic speed control resistance and the throttle setting also need to be specified to complete the setup of a propeller for analysis. Figure 4.1 shows the propeller geometry input screen from Aither.

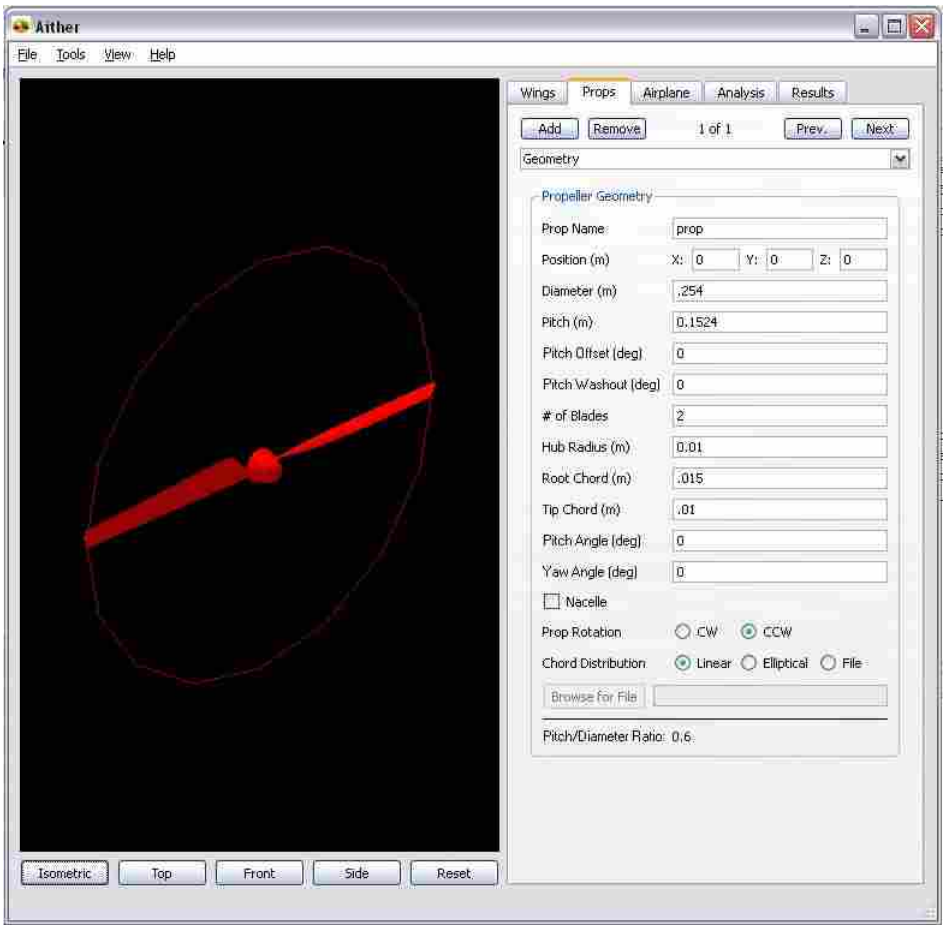

Figure 4.1: Propeller Geometry

4.2.2 Wings

Wings in an Aither aircraft model are defined by the geometry of the wing and the root and tip airfoils. In addition, control surfaces can be added to wing sections. The geometry of a wing is specified using a root and tip chord, wing span, quarter chord sweep angle, root and tip chord twist angles, and dihedral. The root and tip chord twist angles are used for defining geometric washout or washin. The airfoils are defined in exactly the same manner as propeller airfoils. Control surfaces can be added to a wing by specifying the percentage of the wing span, root chord, and tip chord that is taken up by the control surface, as seen in Fig. 4.2.

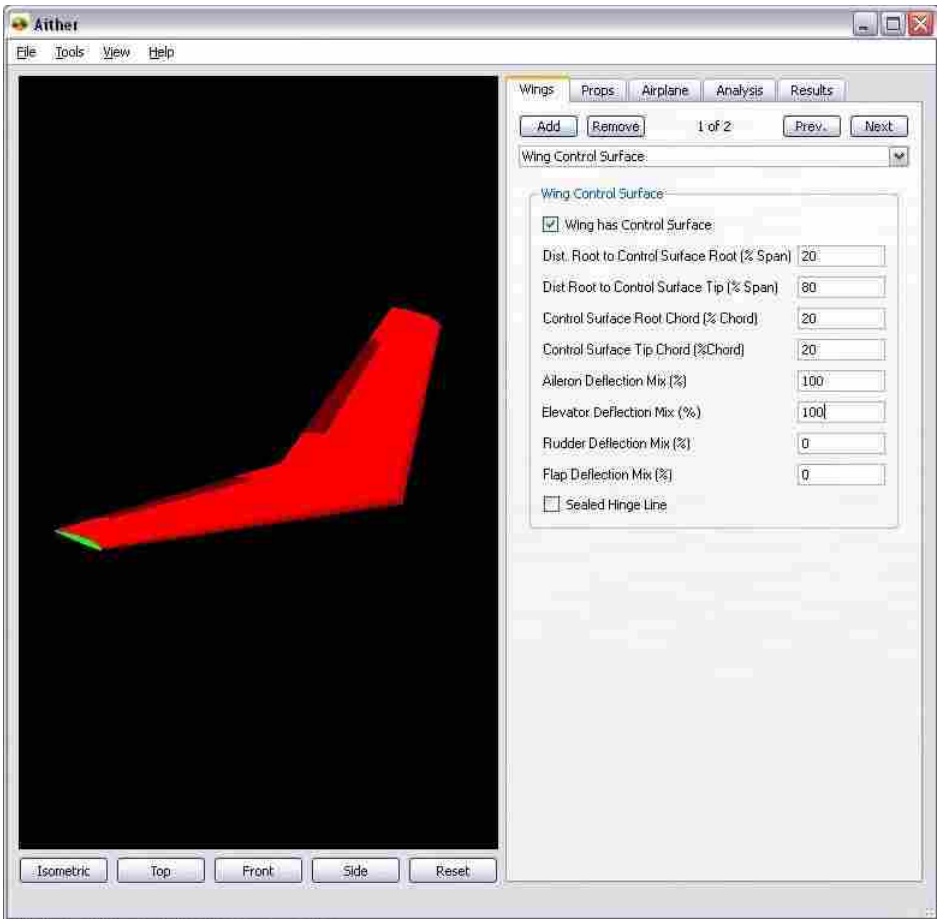

Figure 4.2: Wing Control Surface Input

4.2.3 Aircraft

The setup for the analysis of an Aither aircraft model is completed by setting the input values for the freestream velocity, the aircraft angle of attack and side slip angle, rates of roll, pitch, and yaw, the air density, the aircraft mass and the location of the center of gravity on the aircraft. Also, deflections of any control surfaces can be specified to determine the effectiveness of the control surfaces.

4.2.4 Analysis and Results

Analysis of the aircraft model involves solving the propeller blade element model, then modifying the freestream velocity field and solving the lifting-line model. Results from the program include total lift, drag, and moment coefficients as well as the compo-

nents of these coefficients due to aerodynamic, propeller, and gravitational forces. Propeller results include RPM, thrust, torque, power, and average induced velocity. Thrust and power required are calculated and a drag polar can be constructed. In addition, static stability derivatives can be estimated to allow a first order approximation of the stability of the vehicle.

4.3 Stability

Static stability of the aircraft can be estimated by Aither to predict if the vehicle will be able to fly. Phillips [15] and Roskam [18] provide detailed derivations of both the static and dynamic stability requirements that must be satisfied for safe, reliable flight. A discussion of the stability derivatives available from Aither that are relevant to static stability is provided as a reference to be able to understand the significance of the analysis results. To maintain consistency with previous work, a body-fixed coordinate system is used in Aither. In a body-fixed coordinate system, the positive x-axis points out the nose of the aircraft, the positive y-axis points out the right wing of the aircraft, and the positive z-axis points out the belly of the aircraft toward the earth, as seen in Fig. 4.3.

An aircraft has six degrees of freedom while it is in flight. These are rotation about each of the three axes, and translation in the axial (x), sideslip (y), and normal (z) directions. Typically, stability discussions are divided into longitudinal and lateral stability. Longitudinal stability treats axial and normal translation as well as pitch or rotation about the y-axis. Lateral stability treats translation in sideslip and rotation in roll about the x-axis and yaw about the z-axis.

4.3.1 Longitudinal Stability

Pitch stability is achieved when a change in the angle of attack produces a pitching moment which works to restore the aircraft to its original state. Phillips [15] develops the relation shown in Eq. 4.1,

$$\frac{\partial C_m}{\partial \alpha} < 0.0 \tag{4.1}$$

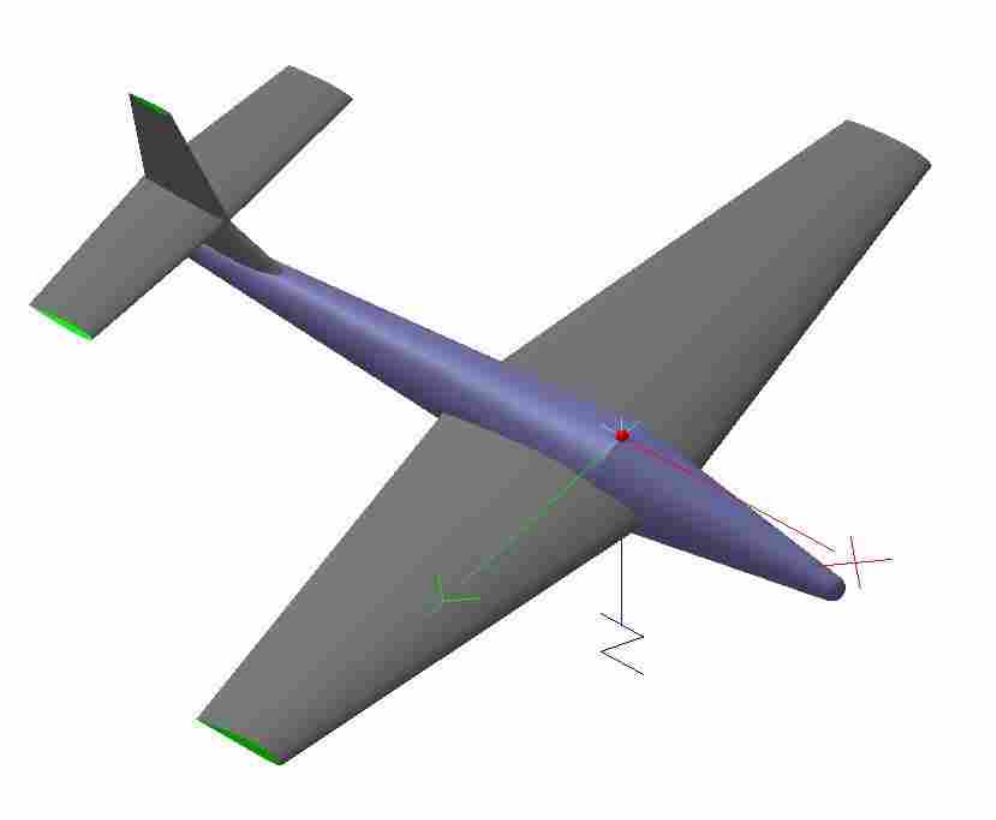

Figure 4.3: Body Fixed Coordinate System

, which shows that a positive change in angle of attack α must result in a decrease in the pitching moment coefficient C_m to maintain pitch stability.

A study of longitudinal stability must include the definition of the static margin σ. The static margin is the distance l_{np} that the center of gravity x_{cg} of the aircraft is ahead of the neutral point x_{np}, normalized by the mean aerodynamic chord c_{mac} as seen in Eq. 4.2. The neutral point of an aircraft is the point about which the total pitching moment acting on the vehicle is independent of the angle of attack. In this respect, it is similar to the aerodynamic center of an airfoil. Experience has shown that the static margin should be in the range of .05 to .15 in order for the aircraft to be stable and controllably flown by a human pilot.

$$\sigma = \frac{l_{np}}{c_{mac}} \tag{4.2}$$

4.3.2 Lateral Stability

Lateral stability is quantified by two stability derivatives which deal with the yaw and roll stability. The yaw stability derivative, shown in Eq. 4.3, must be positive in order for the vehicle to be stable. This equation shows that the change in the total moment about the z-axis, denoted by n, must be able to counter the change in the side slip angle β. Phillips [15] recommends an acceptable range of .06 to .15 for the value of the yaw stability derivative.

$$\frac{\partial C_n}{\partial \beta} > 0.0 \tag{4.3}$$

The roll stability derivative, shown in Eq. 4.4, defines the expected stability in roll about the x-axis. The value of the roll stability derivative must be negative to provide sufficient roll stability and Phillips recommends an acceptable range of -.1 to 0.

$$\frac{\partial C_L}{\partial \beta} < 0.0 \tag{4.4}$$

To augment roll stability, dihedral can be added into the main wings. The effect of dihedral is reflected in the roll stability derivative due to the local changes in angle of attack on opposing wings when the vehicle is rolling. Essentially, as the vehicle rolls, the local angle of attack on the wing which is dropping is increasing while the angle of attack on the opposing wing is decreasing. This leads to asymmetric lift, causing the vehicle to have a tendency to oppose the rolling motion and return to level flight.

Both roll and yaw stability can be increased by incorporating a swept wing with the wings sweeping back from root to tip. Again, local changes in the angle of attack cause asymmetric lift on opposing wing sections in the presence of rolling motion or a side slip angle and the resulting moments are stabilizing.

4.4 Summary

The brief introduction to Aither gives a basic understanding of how the program works and the results that can be expected. The program will give predictions of lift, drag

and yaw forces as well as moments. In addition, stability derivatives are available to aid in the prediction of static stability. These stability derivatives must fall within certain ranges in order for an aircraft to be statically stable. Phillips [15] and Roskam [18] provide excellent sources for more details on stability.

Chapter 5

Results

5.1 Introduction

This chapter describes the prototypes that resulted during this project. Four prototypes were designed, built, flown, and evaluated to see if their performance met the specified criteria for a successful design solution. A brief explanation of each prototype in this evolutionary chain is given along with the information and experience gained from the aircraft construction and flight testing. Details of the final prototype design, construction and flight testing are given along with a comparison of flight performance to predictions from the classic design methods and the aircraft analysis using Aither.

5.2 Prototype 1

5.2.1 Configuration

The Aither model of the first tail-sitter prototype is shown in Fig. 5.1. The details of the configuration of this vehicle are in Table 5.1. The aircraft was constructed as explained in Chapter 4 using EPP foam cores for the wings and the center body section. The center body airfoil profile was a symmetric NACA 0032 and the wing airfoil was the Eppler 186 reflexed airfoil. Rather than the bi-directional fiber tape covering discussed in Chapter 4, the covering applied to this vehicle was a single layer of kevlar composite. The kevlar used on this prototype and throughout the project was non-ballistic grade aramid fabric with a plain weave rated at 1.7 ounces per square yard. The covering was applied using a wet lay-up with an epoxy resin in a vacuum bag. Initially, the entire aircraft was covered in kevlar, but the covering and EPP failed to bond adequately so the entire kevlar covering

Table 5.1: Prototype 1 Configuration

Planform Area (m^2)	.213
Wing Span (m)	1
Aspect Ratio	4.7
Wing Loading (N/m^2)	33.6
Total Mass (g)	730
Center Body Chord (m)	.25
Center Body Span (m)	.254
Wing Root Chord (m)	.25
Wing Tip Chord (m)	.15
Leading Edge Sweep (°)	25
Dihedral (°)	3
Washout (°)	2

was removed and reapplied only to the leading and trailing edges of the wings and all the joints between wing sections. This provided a better bond and reduced the weight of the covering. This aircraft was built as a glider prototype to be used as a proof of concept, so no propulsion system was installed and the control vanes in the propeller shroud were not installed. The elevons on the trailing edges of the main wing were installed to control the vehicle during horizontal flight.

The propeller shroud was constructed using an EPP foam core covered with two layers of kevlar composite. The core was formed by cutting a 1 cm thick sheet of EPP into the shape shown in Fig. 5.2, where all the dimensions shown are in centimeters. The ends of this core were glued together to form an annulus, then the annulus was covered with the epoxy-wetted kevlar material and placed around a cylindrical mold with a diameter of 26.7 centimeters. The entire shroud was vacuumed to the mold and allowed to cure for approximately eight hours. The shroud was designed to allow approximately .5 centimeters of clearance between the propeller tips and the inside wall of the shroud. The foam core of the shroud had a mass of 20.4 grams and the completed shroud had a mass of 74 grams.

5.2.2 Flight Testing

The completed prototype was flight tested using a hand launch and manual control through a Futaba radio console. Flights were made by launching the vehicle in an

Figure 5.1: Prototype 1 Aither Model

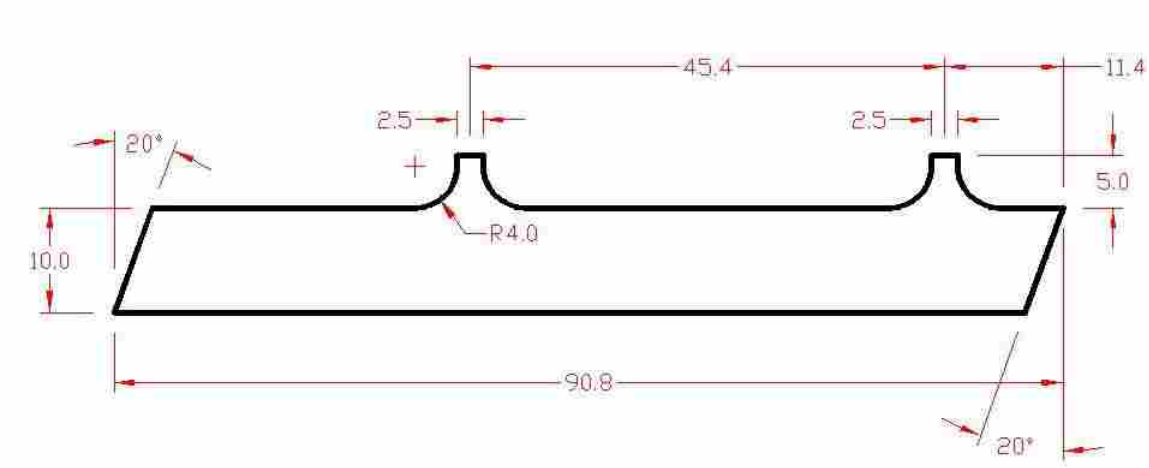

Figure 5.2: Prototype 1 Propeller Shroud Planform

approximately level attitude and piloting the vehicle to a landing in a field at an elevation approximately 25 meters below the launch point. On the day the flight testing was performed, there was no wind. Seven flights were performed, four of which were done with the vehicle center of gravity at 13 cm from the nose and the final three with the center of gravity moved to be approximately 15 cm from the nose. The results from the first four flights showed that the vehicle flew very well, was controllable, and was entirely stable. When intentionally stalled, the wings stayed level, the nose of the aircraft dropped, and the aircraft dove until sufficient flying speed was again attained. In addition, the vehicle tracked in a very straight line with no tendency to deviate from its course in yaw. Response to the elevons in roll and pitch was acceptable and allowed the vehicle to be adequately controlled. The center of gravity was moved back for the final three flights to verify the Aither prediction of the stability of the aircraft. When the vehicle was balanced with the center of gravity at 13 centimeters from the nose, the predicted static margin was 7.2%. With the center of gravity moved back to 15 centimetes from the nose, the predicted static margin was 0.0%, or $l_{np} = 0$. The three flight tests with the center of gravity moved back showed that the aircraft was still flyable, but the flying qualities were much worse than with the previous center of gravity location. The aircraft would pitch up rapidly on launch and was just barely stable in pitch. Very small control inputs produced large changes in pitch of the vehicle. The stall response was similar to the previous behavior, but it was much easier to enter the stall. When stabilized in pitch, the aircraft response to roll inputs was essentially unchanged and it still tracked in a very straight line.

5.2.3 Prototype 1 Summary

The flight tests of this prototype showed that the concept was viable in horizontal flight and that the Aither stability predictions were reliable. The aircraft was controllable, stable, and flew well if balanced with an adequate static margin. However, calculations showed that balancing the aircraft properly with the propulsion system installed was impossible. Balancing the aircraft would have required placing the battery further forward than was physically possible, locating it outside the actual airframe. In addition, flight testing also showed that, even though the aircraft never suffered a crash, the kevlar composite

used to reinforce the wing joints and the leading and trailing edges of the wings began to separate from the foam core after several landings. The shroud design proved to be robust and did not suffer any damage.

5.3 Prototype 2

5.3.1 Configuration

The second prototype was designed with two major planform changes over the previous prototype. The first was a change in leading edge sweep angle from 25 degrees to 30 degrees. This change shifted the neutral point of the aircraft further aft, which helped to achieve proper balance with the propulsion system installed. The second change was decreasing the chord length of the center body of the aircraft and shifting the shroud forward, as seen in the Aither model in Fig. 5.3. To maintain adequate wing area, the root and tip chords of the wings were increased by 5 centimeters each as well. These changes allowed the motor, propeller, propeller shroud, and contol vanes to be placed further forward on the aircraft, which also helped achieve proper balance of the vehicle. Table 5.2 contains the details for the second prototype configuration.

The aircraft body was constructed using a symmetric NACA 0025 airfoil, slightly thinner than in the previous prototype. The airfoil for the body section was chosen to be just thick enough to allow components and the payload to be inserted in the body. Also, on this prototype the covering used was bi-directional fiber tape rather than kevlar composite. The tape was applied to the leading and trailing edges of the wings and along all the wing joints. The shroud design was not changed, but a new shroud was built. The new shroud had a mass of 90.5 grams, an increase of 16.5 grams compared to the first shroud. The propulsion system selected and installed on the aircraft consisted of an Axi 2814/10 brushless electric motor with a Hacker Master 70-B electronic speed control (ESC) and a ThunderPower 4000 mAh 11.1 volt 3 cell lithium polymer battery pack. The propeller attached to the motor was a MasterAirscrew G/F 3 Series 10x6 inch propeller. The motor was mounted in a pusher configuration and the ESC and battery were mounted in compartments cut into

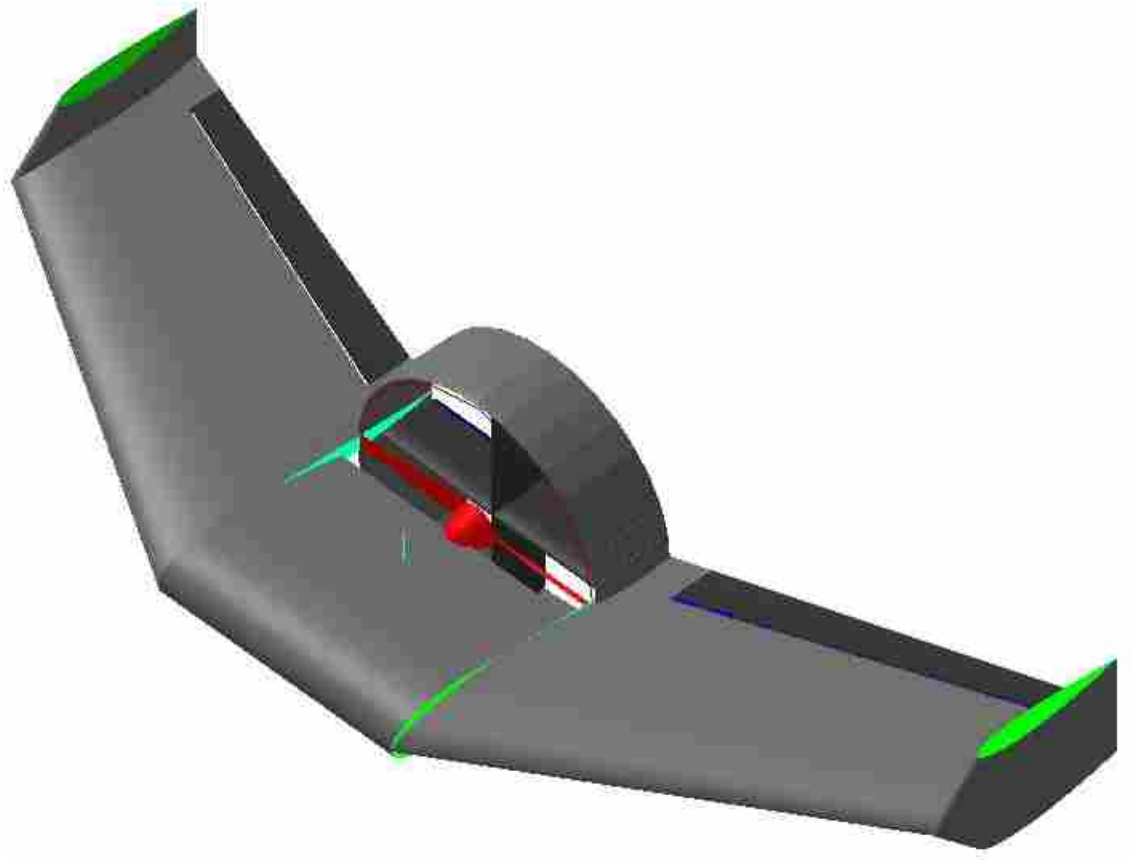

Figure 5.3: Prototype 2 Aither Model

the foam of the center body section. The control vanes in the propeller shroud were not installed on this vehicle.

5.3.2 Flight Testing

Flight testing for the second prototype was divided into two parts and was accomplished using manual control. First, horizontal flight testing was conducted with the aircraft. This involved three gliding flights and seven powered flights over several days. The gliding flights were done to ensure the aircraft was balanced properly. During all three flights, the airplane was consistently stable and was controllable in roll, pitch, and yaw. Compared to the previous prototype, glide performance was similar except for the total glide distance. The glide distance was reduced because this aircraft was about 150 grams heavier with a similar wing area, leading to a higher wing loading. In the first five powered

Table 5.2: Prototype 2 Configuration

Planform Area (m^2)	.237
Wing Span (m)	1
Aspect Ratio	4.21
Wing Loading (N/m^2)	36.2
Total Mass (g)	875
Center Body Chord (m)	.20
Center Body Span (m)	.254
Wing Root Chord (m)	.30
Wing Tip Chord (m)	.20
Leading Edge Sweep ($^\circ$)	30
Dihedral ($^\circ$)	3
Washout ($^\circ$)	2

flights flown after glide testing, a problem with the propulsion system was encountered. The aircraft would fly well for approximately three minutes, then the motor would cut and the airplane had to be glided in for a landing. Initially, the problem was suspected to be overheating of the motor or ESC due to the large diameter propeller. After the first two flights, the propeller was changed from a 10x6 inch to a 9x4.5 inch to see if the smaller diameter and lower pitch would aleviate the problem. One more flight was flown, but the problem was not fixed and the motor still cut out after approximately four and a half minutes of powered flight. The ESC was hot to the touch after all of the preceding powered flights, so overheating was still suspected. The ESC was mounted outside of the foam center body in the airstream for the final flights to test that theory since, with the ESC mounted inside the EPP foam, there was no cooling airflow past the device. This resulted in two complete flights of 13 minutes 11 seconds and 14 minutes 50 seconds, respectively. Premature shutdown of the motor was eliminated by mounting the ESC outside the body where it was cooled by the passing airflow.

For the last five powered flights, the battery voltage was recorded both before and after the flight. Also, the flight time was recorded automatically by the Futaba radio console by setting the timer to be activated whenever the throttle setting was greater than 7%. The amount of battery capacity used during each flight was available from the battery charger and was also recorded. These values were used to calculate the average battery voltage,

Table 5.3: Prototype 2 Horizontal Flight Test Data

Flight	Propeller (inch)	Time (min:sec)	Capacity Used (mAh)	Voltage (V)	Current (A)	Power (W)
1	10x6	3:12	739	12.14	13.9	168
2	10x6	2:09	580	12.1	16.2	196
3	9x4.5	4:28	1120	12.1	15.0	183
4	9x4.5	13:11	3820	11.14	17.4	194
5	9x4.5	14:50	3600	11.34	14.6	165

power consumption and current draw from the battery for each flight. Table 5.3 shows that the average power draw for all flights was 181 watts and the average current was 15.4 amps.

The second part of flight testing was vertical flight testing. For the initial test, the aircraft was restrained to allow only vertical motion and was conducted indoors. Vertical testing with this prototype proved that the propulsion system produced inadequate thrust to allow vertical flight. The vehicle would become airborne in ground effect only, but the thrust-to-weight ratio was inadequate to allow a vertical climb or hover out of ground effect. Because the vehicle did not have adequate thrust, further testing for controlablity in vertical flight was not performed.

5.3.3 Prototype 2 Summary

The second prototype also proved to be a viable design in horizontal flight, but it failed in vertical flight due to inadequate thrust. The plane was stable in horizontal flight and responded well in pitch. The roll rate was very fast compared to the previous prototype, and care had to be exercised while flying to maintain control. The airframe suffered one crash during flight testing, but was easily repaired and continued to fly. The overheating of the ESC showed that this component needed to be mounted in a location where there was adequate airflow for cooling. Another issue that arose during construction and flight testing was the lack of physical space available for a payload, as shown in Fig. 5.4. In addition, the power required for horizontal flight was higher than desired, resulting in a flight time that was shorter than desired as well.

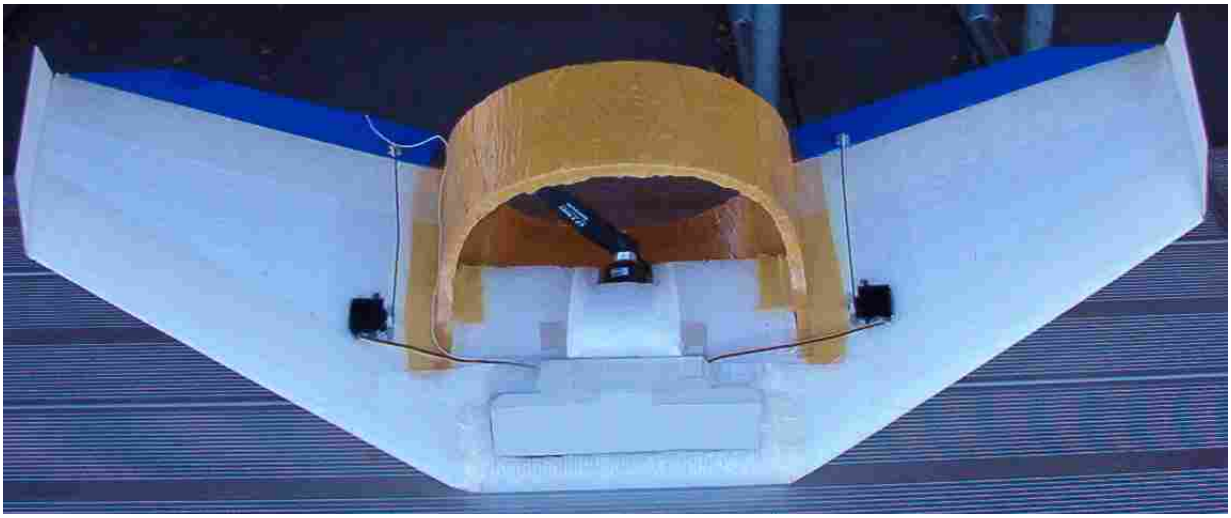

Figure 5.4: Prototype 2

5.4 Prototype 3

5.4.1 Configuration

Experience with the previous prototypes caused several major changes to be made in the design of the third aircraft. The sweep of the wings was reduced back to 25 degrees from 30 degrees to reduce the roll rate and make the aircraft easier to fly. The center body section was increased in chord by 13 centimeters and decreased slightly in span by 1 centimeter to allow more space for component and payload placement. The center body was trimmed along the trailing edge to allow clearance for the propeller, producing a blunt trailing edge. Also, the propulsion system was upgraded by changing the electric motor to a larger and more powerful Mega ACn 22/30/3 brushless electric motor. The resulting configuration is shown in Fig. 5.5 and the details of this design are in Table 5.4.

The configuration of this prototype was modified twice after performing two powered flight tests. All of the modifications were to the propeller shroud and were made in an effort to streamline the structure for reduced drag. The modifications will be explained here and their effects will be discussed in the following section on Flight Testing. The shrouds used on the previous prototypes were all made using a sheet of EPP with a constant thickness of one centimeter. The chord length of the shroud was 10 centimeters, so the airfoil

Table 5.4: Prototype 3 Configuration

Planform Area (m^2)	.267
Wing Span (m)	1
Aspect Ratio	3.67
Wing Loading (N/m^2)	46.0
Total Mass (g)	1251
Center Body Chord (m)	.33
Center Body Span (m)	.245
Wing Root Chord (m)	.30
Wing Tip Chord (m)	.20
Leading Edge Sweep (°)	25
Dihedral (°)	3
Washout (°)	2

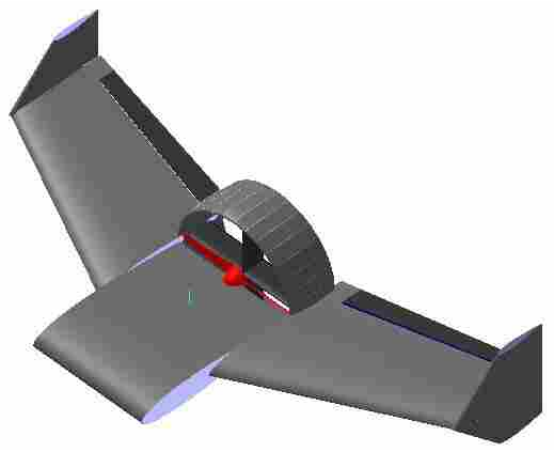

Figure 5.5: Prototype 3 Aither Model

profile of the shroud was a rectangle with a thickness of 10% of the chord. This profile is aerodynamically very inefficient, so the shroud was changed on the third protoype after two flights. The new shroud was made with a foam core having a symmetric NACA 0009 airfoil cross section. The new shroud was covered with the bi-directional fiber tape rather than the kevlar composite to reduce construction time and structure weight. The construction time was reduced by several hours and the total mass of the duct was reduced to 50 grams using the tape covering. Two flight tests were performed, and the new shroud was found to be to flexible and broke away very easily. It was removed and rebuilt. The core was again a

NACA 0009 airfoil cut from EPP foam with a chord of 10 centimeters. The covering was changed to two layers of kevlar fabric and the shroud was formed using a cylindrical mold and a vaccuum bagging process. The structure of this shroud was much more ridgid and was found to be acceptable. The mass of the final shroud was 70 grams, equivalent to the original shroud but with a more aerodynamic profile.

For vertical flight testing, control vanes were installed in the propeller shroud. Each of the four vanes had a chord of 5 centimeters and a span of 13 centimeters and was constructed using a flat 3/32 inch balsa wood core covered with colored packaging tape for reinforcement. A small diameter tube was adhered to the leading edge of the vanes and a solid wire passed through the tubes to attach each vane to the aircraft. The vanes were installed with three centimeters of clearance behind the propeller and were hinged at the leading edge of the vane. The two vertical vanes were coupled to a single rudder control and were not allowed to move independently of each other. The horizontal vanes were coupled to separate controls and could move independently to functioned as elevons.

5.4.2 Flight Testing

Five powered flight tests were performed with the third prototype, two with the original rectangular shroud and three with the new kevlar-covered modified shroud. Table 5.5 shows a reduction of approximately 50% in the power required to fly the aircraft after the modified shroud was attached. Two different propellers were also tested to determine which would yield the best flight performance. The 10x6 inch propeller provided more top speed, but required more power from the battery. The top speed of the airplane was reduced significantly when the 10x4 inch propeller was used, and the aircraft flew with an extremely nose-high attitude until sufficient down elevator trim was added to the elevons.

Many flights were made with the vehicle in vertical flight to determine the ability of the aircraft to hover and be controllable. Four flights were made with the vehicle restrained to allow only vertical movement, using two different propellers. These tests were done to determine if the vehicle would be able to hover. The results from the tests, quantified in Table 5.6, showed that the aircraft produced sufficient thrust to hover and accelerate verti-

Table 5.5: Prototype 3 Horizontal Flight Test Data

Flight	Propeller (inch)	Time (min:sec)	Capacity Used (mAh)	Voltage (V)	Current (A)	Power (W)
1	10x6	9:06	3572	11.5	13.9	271
2	10x6	10:39	3745	11.1	16.2	235
3	10x6	11:01	1664	11.5	15.0	104
4	10x6	13:55	2517	11.25	17.4	122
5	10x4	15:47	3316	11.0	14.6	139

Table 5.6: Prototype 3 Vertical Flight without Control Vanes

Flight	Propeller (inch)	Time (min:sec)	Capacity Used (mAh)	Voltage (V)	Current (A)	Power (W)
1	10x6	0:34	216	12.3	23	283
2	10x6	3:18	1520	11.9	27.6	327
3	10x4	1:08	405	12.3	21.4	262
4	10x4	1:47	628	12.3	21.2	260

cally using both propellers. However, observation showed that the vertical acceleration and total thrust were less using the 10x4 inch propeller as compared to the 10x6 inch propeller and that the available thrust using either propeller was just barely enough to overcome the weight of the airplane.

Next, the control vanes were installed in the propeller shroud and flight tests were performed to determine if the vehicle would be controllable in vertical flight. Two initial tests showed that the vehicle responded well to the elevator and rudder commands, but the roll response was inadequate to counter the torque produced by the propulsion system. The aircraft would begin to slowly rotate about the x-axis in roll, and the aileron vanes were unable to produce enough counter-torque to reverse the roll. The control vanes were modified by doubling the chord to 10 centimeters, and the tests were repeated. The roll control was improved but was still insufficient to counter the motor torque. The control vanes were modifed a second time by switching to a foam core covered with bi-directional fiber tape. The foam core was cut to a symmetric NACA 0009 airfoil with a chord of 12 centimeters and the hinge line was changed to approximately the quarter chord of the vanes. This modification left .5 centimeters of clearance between the propeller and the

control vanes. Also, the coupling of the two rudder control vanes was changed by adding an additional servo and connecting each vane to a seperate servo. This allowed the vanes to deflect in the same direction when used for rudder control, and to deflect in opposite directions to augment the elevons for roll control. Four flight tests were performed with the modified control vanes. The quantified results of these tests are shown in Table 5.8. Roll control was improved sufficiently and the vehicle was able to rotate about the roll axis in either direction on command. However, the addition of a servo and excess structure weight caused the aircraft to be too heavy to accelerate vertically. Controlled hover in ground effect was possible, but the airplane would not climb vertically. Equation 5.1 shows a relation that was developed to aid in the sizing of the control vanes. This equation defines an area fraction f_{area} as a ratio of the total control vane area to the propeller disk area. The area of a single control vane A_{vane} is multiplied by the total number of vanes n_{vanes} to get the total control vane area. The maximum lift coefficient $C_{l,max}$ of the control vanes is added to account for the aerodynamic efficiency of the vane cross section. Performing calculations using this equation for the three different control vane sizes yielded the results shown in Table 5.7. This data suggests that the area fraction f_{area} should be approximately .83 or greater in order to have sufficient control. In the final configuration shown in Fig. 5.6, the control vane area decreased slightly from the previous configuration. This was due to the trimming of the control vanes to allow for full movement without binding on each other or on the sides of the propeller shroud. However, the decrease in size was mitigated by the improvement in aerodynamic efficiency from using a symmetric NACA 0009 airfoil shape rather than a flat plate.

$$f_{area} = \frac{4 n_{vanes} A_{vane} C_{L,max}}{\pi D^2} \tag{5.1}$$

5.4.3 Prototype 3 Summary

The third prototype provided valuable flight test data that was used to analyze the aircraft performance. Horizontal flight testing showed that the airplane still used more power than was desired, but roll control was improved over the second prototype. The ve-

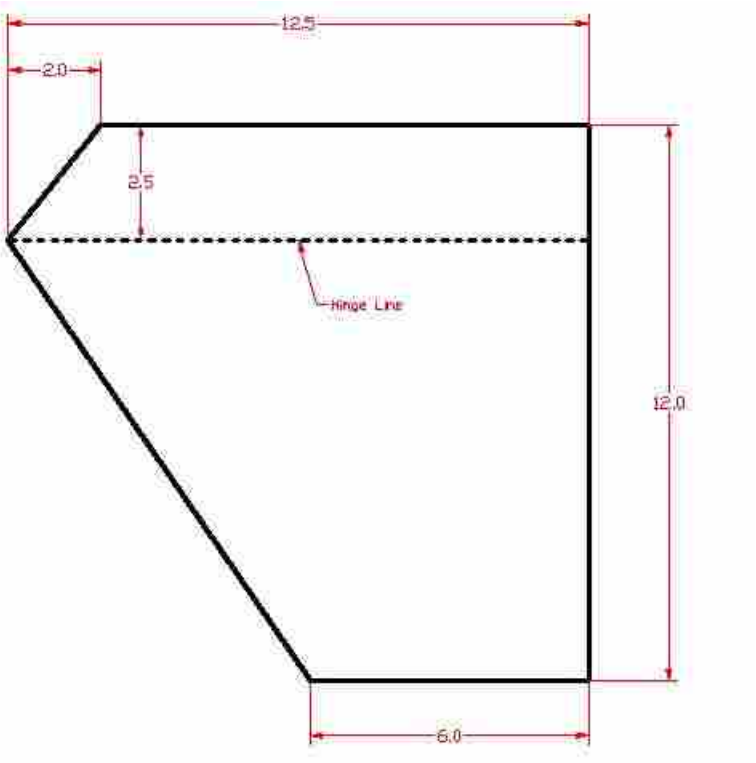

Figure 5.6: Final Control Vane Configuration

Table 5.7: Control Vane Sizing

Configuration	**Vane Area (cm^2)**	**Vane Quantity**	**Vane $C_{L,max}$**	**Propeller Diameter (cm)**	**Area Fraction**
Flat Plate	71.5	4	.7	25.4	.40
Flat Plate	136.5	4	.7	25.4	.75
NACA 0009	117	4	.9	25.4	.83

Table 5.8: Prototype 3 Vertical Flight with Control Vanes

Flight	**Propeller (inch)**	**Time (min:sec)**	**Capacity Used (mAh)**	**Voltage (V)**	**Current (A)**	**Power (W)**
1	10x6	2:38	1335	11.9	30.4	362
2	10x6	1:59	1052	12.1	31.8	387
3	10x4	1:00	417	12.3	25	308

hicle suffered one significant crash due to pilot error during horizontal flight testing. This required repairs to the airframe, which increased the structure mass and reduced the performance in vertical flight. Vertical flight tests showed that without control vanes installed, the aircraft would hover and climb vertically. However, the addition of control vanes and the modification of the control system to allow roll control in hover reduced the maximum thrust to a point that wouldn't allow the aircraft to climb. The area fraction of the control vanes was also studied to aid in determining the necessary size of the control vanes.

5.5 Prototype 4

The fourth prototype was designed with two changes. First, the center body section was significantly reduced in span and the chord length was increased, as seen in Fig. 5.7. This was done to reduce the structure weight while still allowing proper balance. Second, the shroud was moved further aft to allow the center section of the airplane to taper completely at the trailing edge in front of the propeller rather than being blunted as in the previous prototype. In addition, working with the two previous prototypes demonstrated that the structure weight of the vehicle was critical and needed to be carefully monitored during construction. As this was the final prototype, more detail is provided on the design, construction and flight testing of this vehicle in the following sections than was presented for the previous prototypes.

5.5.1 Preliminary Design

Following the design steps laid out in Chapter 4, an initial weight estimate for the aircraft was made using a structure weight fraction of $X_{str} = .35$. Experience has shown that a structure weight fraction in the range of .4-.5 is usually adequate for a flying wing UAV. However, since the weight of a VTOL aircraft is critically important, a design goal of .35 was chosen. Table 5.9 shows the initial breakdown of the total mass and weight of the vehicle.

Due to the absence of a conventional empenage, a reflexed airfoil with a positive pitching moment was used in order to provide pitch stability. The Eppler 186 airfoil was

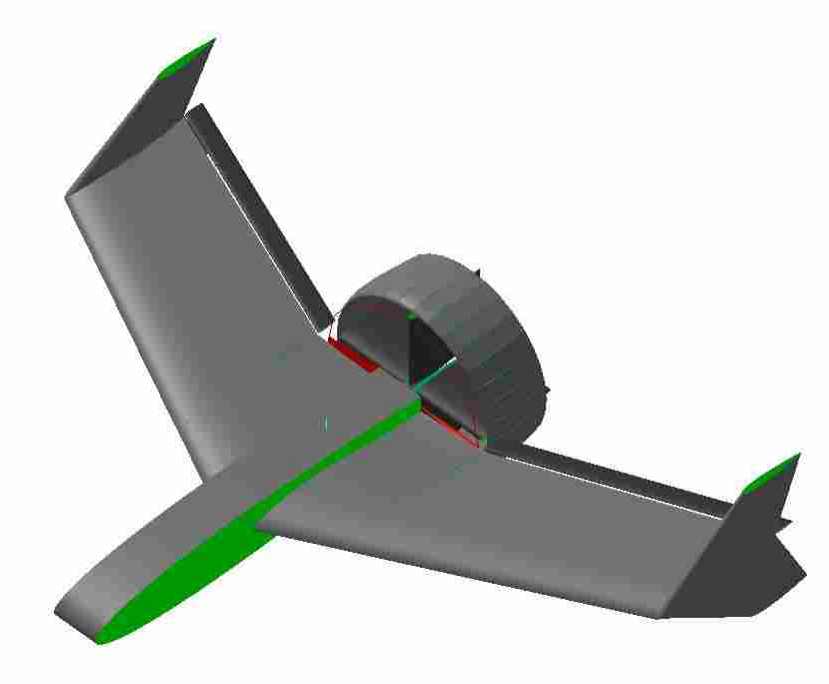

Figure 5.7: Prototype 4 Aither Model

Table 5.9: Preliminary Weight Estimate

Item	**Quantity**	**Mass (kg)**	**Weight (N)**	**Weight Fraction**
Battery	1	.270	2.65	.202
Propulsion	1	.290	2.84	.217
Servos	4	.020	.78	.060
Electronics	1	.030	.029	.022
Structure	1	.468	4.60	.350
Payload	1	.200	1.96	.149
Total Aircraft	1	1.338	13.13	1.0

chosen for use at both the root and tip sections of the entire wing. The characteristics of this airfoil predicted by XFoil at a Reynolds number of 170000 are shown in Fig. 5.8 along with the profile of the airfoil itself. The predicted maximum lift coefficient of .967 was reduced by 20% to make the initial adjustment for a finite wing and the wing configuration was calculated. The input parameters and resulting configuration values are shown in Table 5.10.

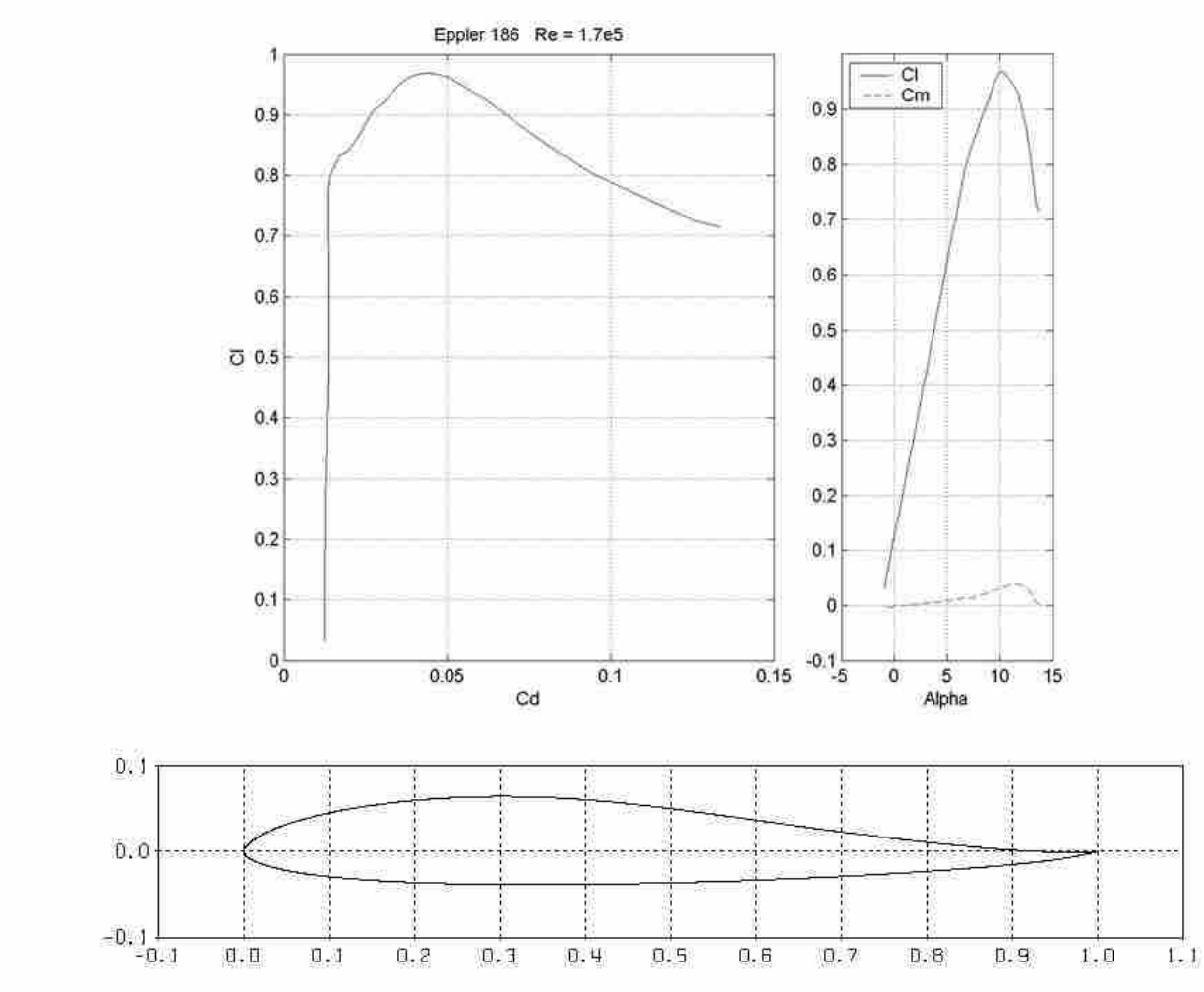

Figure 5.8: Eppler 186 Airfoil, Re = 170,000

Using the airfoil characteristics and published data from Anderson [14], the zero lift drag coefficient $C_{D,0}$ was estimated to be .0122 and the induced drag factor δ was estimated to be .05. These values were used to calculate the aircraft drag polar and to estimate the thrust and power required for flight.

The vertical stabilizers or winglets were designed next, with the results shown in Table 5.11. In these calculations, the height h_{vt} of the winglet referred to the tip-to-tip distance of the stabilizer since it extended both above and below the wing surface.

The next step in the preliminary design was the selection of a propulsion system. Using the propulsion system analysis presented in Chapter 3 and the results of previous flight tests, it was decided to use a 10x6 inch propeller. The motor was selected from com-

Table 5.10: Preliminary Wing Configuration

Parameter	**Value**
Aspect Ratio	3.9
Taper Ratio	.667
Leading Edge Sweep (°)	25
Geometric Twist (°)	3
Wing Loading (N/m^2)	51.2
Wing Area (m^2)	.256
Wing Span (m)	1.0
Root Chord (m)	.300
Tip Chord (m)	.200
Mean Aerodynamic Chord (m)	.260
Spanwise MAC Offset (m)	.174
Aerodynamic Center (m)	.233

Table 5.11: Stabilizer Sizing

Parameter	**Value**
Volume Fraction	.016
Aspect Ratio	1.38
Taper Ratio	.5
Leading Edge Sweep (°)	56.3
Total Stabilizer Area (m^2)	.065
Winglet Height (m)	.20
Winglet Root Chord (m)	.200
Winglet Tip Chord (m)	.100

mercially available products which are rated to produce thrust in excess of the estimated weight of the aircraft. Specifically, the Mega ACn 22/30/3 motor was selected. Experimental data compiled by Wergeland [19] suggests that this motor and propeller combination should produce approximately 1.6 kilograms of thrust under static conditions with an operating voltage of 10.4 volts. This static thrust would produce a thrust-to-weight ratio of 1.2.

The battery selected for the aircraft was sized using Eq. 3.28 and a safety factor of 2.0 to ensure sufficient battery capacity. The selected battery was the 3-cell 11.1 V lithium

polymer ThunderPower 4000 mAh. The selected battery not only had sufficient capacity, but it was rated at a high discharge rate which was required for hovering flight.

Materials for the aircraft were selected to ensure proper flight, ease of construction, durability, and ease of repair. The cores of the wings and the propeller shroud were Expanded Polypropylene (EPP) with a density of 1.3 pounds per cubic foot. The EPP foam core of the wings was covered with bi-directional fiber tape. A spray adhesive was applied to the foam core before application of the tape to strengthen the adhesion of the tape to the foam. This covering increased the stiffness of the wings while still allowing some flexibility to absorb energy from rough handling. The propeller shroud foam core was cut to a NACA 0010 profile and was covered with two layers of non-ballistic grade Kevlar fabric rated at 1.7 ounces per square yard. An epoxy resin was used as a binder and the shroud was constructed using a wet lay-up in a vacuum bag. This covering greatly increased the structural stiffness of the shroud, which was necessary since the shroud served as a structural component for attachment of the control vanes and as a propeller shield in the event of tip-over or crash. The control vanes were constructed with a foam core covered with bi-directional fiber tape as well.

After selecting the materials, a refined weight analysis was conducted to verify that the weight of the structure was within the preliminary allotment. Table 5.12 shows the final estimate of the weight of the vehicle. The aircraft planform was created by iterating on the weight and balance calculations of the aircraft to make sure the vehicle weight would be within the limit for the structure and that the physical layout of the vehicle would allow it to be balanced for flight. The modified flying wing planform was created to allow adequate clearance for the propeller and propeller shroud while allowing the center wing section to taper completely. In this configuration, each semispan is divided into an inboard and an outboard section. The inboard section spans from the vehicle centerline to the junction of the wing with the propeller shroud. This section has no sweep on the trailing edge to allow clearance for the propeller. The outboard section continues from the junction to the wing tip.

The refined weight estimate showed that the preliminary weight estimates were adequate and that the vehicle design weight would allow a thrust-to-weight ratio of 1.28.

Table 5.12: Final Weight Estimate

Component	**Volume** (cm^3)	**Density** (g/cm^3)	**Mass** (g)	**Weight** (N)
Left Outboard Foam Core	1109	.0224	24.9	.24
Left Inboard Foam Core	459	.0224	10.3	.1
Body Foam Core	2522	.0224	56.6	.55
Right Inboard Foam Core	459	.0224	10.3	.1
Right Outboard Foam Core	1109	.0224	24.9	.24
	Area (cm^2)	**Area Density** (g/cm^2)		
Left Outboard Covering	1567	.0167	26.2	.26
Left Inboard Covering	543	.0167	9.1	.09
Body Covering	1490	.0167	24.9	.24
Right Inboard Covering	543	.0167	9.1	.09
Right Outboard Covering	1567	.0167	26.2	.26
	Quantity	**Unit Mass** (g)		
Propeller Shroud	1	70	70	.69
Motor	1	220	220	2.16
Speed Control	1	70	70	.69
Servo 1	1	18	18	.18
Servo 2	1	18	18	.18
Servo 3	1	18	18	.18
Servo 4	1	18	18	.18
Electronics	1	30	30	.29
Battery	1	265	265	2.6
Miscellaneous Structure	1	100	100	.98
Payload	1	200	200	1.96
Total			1249.2	12.26

With the refined estimate, the structure weight fraction was .31 compared to the initial estimate of .35.

5.5.2 Aircraft Analysis

The aircraft configuration shown in Fig. 5.9 was input into Aither for analysis. The model was constructed using six wing sections to build the body and wings. The body of the aircraft was modeled with two symmetric wing sections consisting of a NACA 0010 airfoil with a chord of 55 centimeters and a span of 7 centimeters. The inboard sections

Table 5.13: Motor Specifications

Motor	Mega ACn 22/30/3
RPM/Volt	1850
No Load Current (A)	1.76
Armature Resistance (Ohms)	.016
Mass (kg)	.22
Gear Ratio (1:xx)	1
Speed Control Resistance (Ohms)	.002
Throttle Setting (%)	70

of the wings were located symmetrically about the centerline of the vehicle. The inboard sections had a semi-span of 10.47 centimeters, a root chord of 28.37 centimeters and a tip chord of 23.48 centimeters. The leading edges of the inboard wing sections were swept back at 25 degrees and the trailing edges had no sweep. The outboard sections of the main wing were modeled using root and tip chords of 23.48 centimeters and 20.0 centimeters, respectively, and a semispan of 36.03 centimeters. The leading edges were also swept back at 25 degrees to maintain a continuous linear leading edge. Figure 5.9 shows these dimensions on the planform of the aircraft. Dihedral and washout were added into the outboard wing sections as well, with the dihedral set at three degrees and the washout at two degrees. The winglets at each wingtip tip were modeled with two symmetric wing sections, one above the wing and one below the wing. These wing sections aerodynamics were modeled using NACA 0009 airfoil data. The root and tip chords were 20 centimeters and 10 centimeters respectively and the semi-height was 10 centimeters to give a total span of 20 centimeters for the entire winglet assembly, as seen in Fig. 5.9. The propeller shroud was modeled using 32 wing segments with a NACA 0009 airfoil. Each segment had a constant chord of 10 cm and a span of 2.48 cm. The aircraft model was completed by placing the four control vanes in the propeller shroud. These wing sections had a constant chord of 12 cm and a span of 11 cm.

The propeller modeled in Aither was a standard 10x6 inch model aircraft propeller. The input values for the motor and battery are shown in Tables 5.13 and 5.14. To complete the entire aircraft model, the mass of the vehicle was set to 1.3 kilograms and the center of gravity was specified to be at 42.5 centimeters aft of the nose.

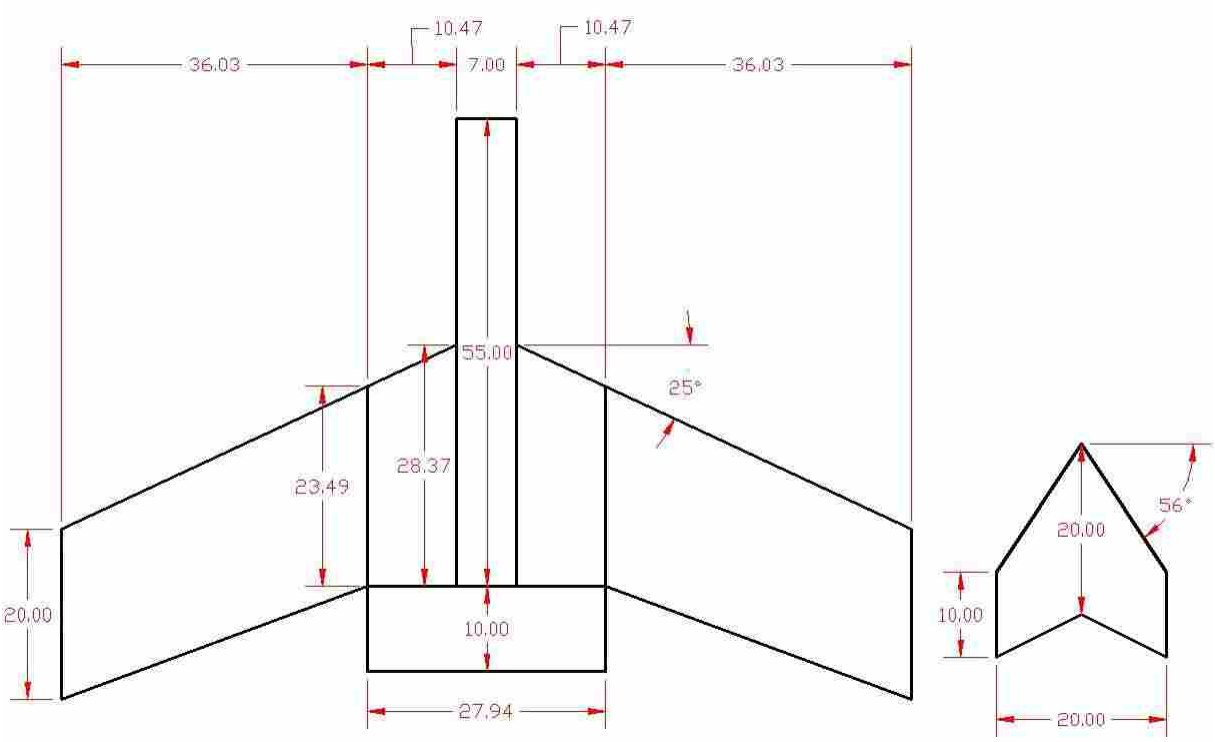

Figure 5.9: Prototype 4 Planform

Table 5.14: Battery Specifications

Battery	ThunderPower 4000 mAh
Capacity (mAh)	4000
Voltage (A)	11.1
Impedance (Ohms)	.099
Mass (kg)	.265
Discharge Rating (C)	12

Analysis of the model predicted that the aircraft would cruise at 15 m/s at an angle of attack of 4.9 degrees, resulting in a lift-to-drag ratio of 11.2. The predicted power consumption was 138 watts and the predicted flight time in horizontal flight was 15.4 minutes. Aither predictions of power and thrust required versus airspeed are shown in Figs. 5.10 and 5.11 along with the predictions from the classic design method. Comparison of the Aither predictions to those from the classical design method showed that Aither consistently predicted more thrust and power would be required due to higher drag. The predicted drag

polars are shown in Fig. 5.12 and the lift-to-drag ratios are plotted against airspeed in Fig. 5.14. Aither predicted a maximum lift-to-drag ratio of 11.3 at a velocity of 14 m/s while the classical design method predicted a maximum of 15.5 at a velocity of 16.5 m/s. Aither predictions for the lift and drag coefficients of the tail-sitter through a range of 180 degrees are shown in Fig. 5.13. The predictions for these coefficients follow the trends given for a tail-sitter published by Knoebel, etal [20], and showed that the aircraft had the potential to function well as a VTOL UAV. Table 5.15 shows the predictions for the aircraft static margin and the stability derivatives when the aircraft center of gravity was placed 45 centimeters aft of the nose. The static margin prediction of 11.15% was well above the minimum of 5% so the aircraft was predicted to be controllable in horizontal flight. The stability derivatives predicted that the aircraft would be stable in roll and pitch, but might suffer from instability in yaw.

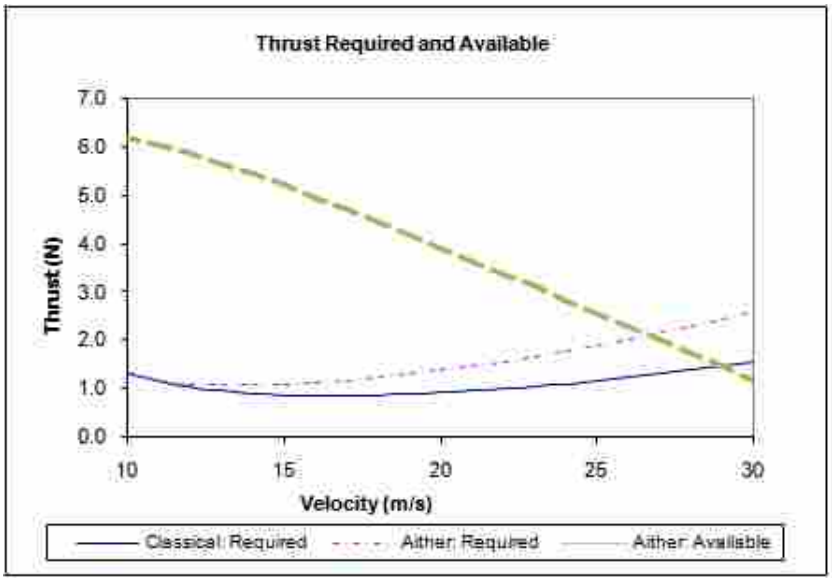

Figure 5.10: Thrust Predictions

5.5.3 Construction

The aircraft was built in a manner similar to the previous prototypes. The wings and body consisted of an EPP foam core covered with fiber tape. The shroud was a NACA

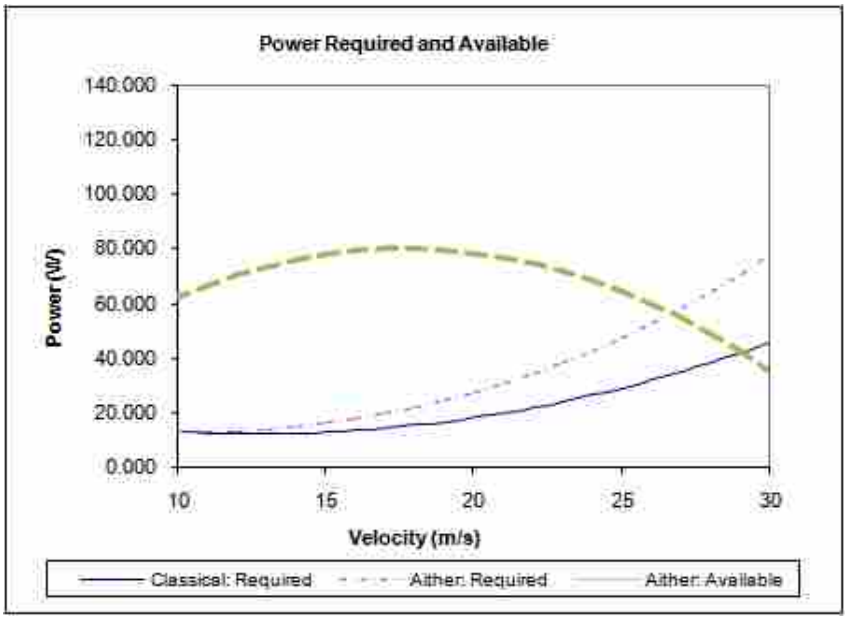

Figure 5.11: Power Predictions

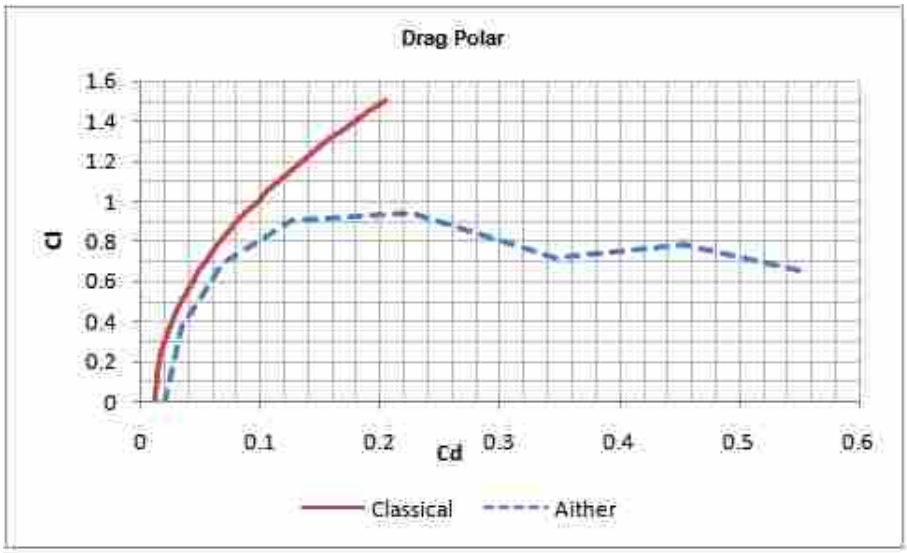

Figure 5.12: Drag Polar

0010 EPP foam core with two layers of kevlar composite covering. The wings and body were joined using an epoxy adhesive, then coated with a spray adhesive before the fiber tape covering was added. Carbon tubes with an outside diameter of .635 cm were inserted at the joints of the inboard wing sections with the outboard wing sections and extended 12

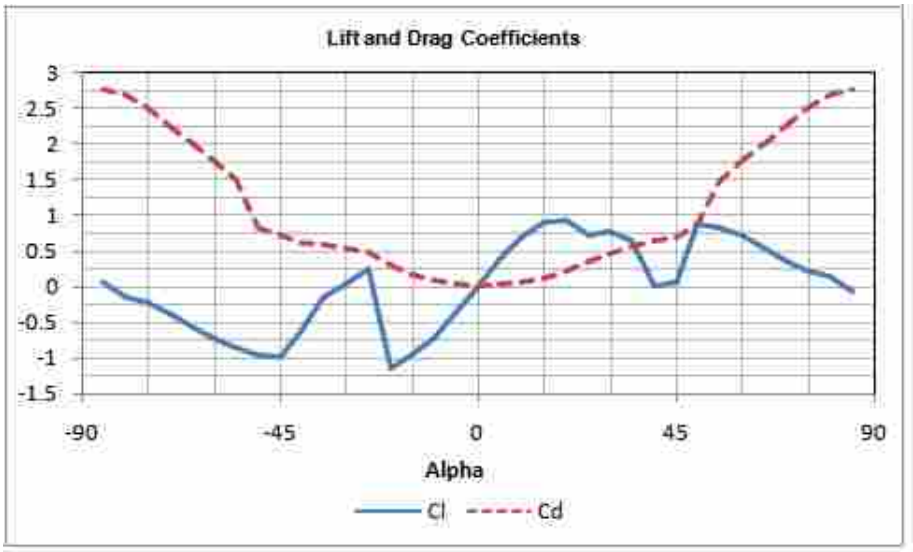

Figure 5.13: Lift and Drag Coefficients

Table 5.15: Static Margin and Stability Derivatives

Item	**Value**	**Prediction**
Static Margin	11.15%	Longitudinally Stable
$\partial C_m/\partial\alpha$	-.0012	Stable in Pitch
$\partial C_n/\partial\beta$	-.0023	Unstable in Yaw
$\partial C_L/\partial\beta$	-.0023	Stable in Roll

centimeters past the trailing edge of the wings. These were used to attach the propeller shroud to the airframe. The motor, battery, ESC, and servos were laid out as shown in Fig. 5.15. Two servos were placed in the propeller shroud, one on the top and one on the bottom. These two servos were configured to make the vertical control vanes move in the same direction for rudder commands and in opposite directions for aileron commands. The two servos placed in the wing were connected to the horizontal control vanes inside the propeller shroud and to the elevons at the trailing edge of the wings. These servos were configured to make the horizontal control vanes and the elevons move in the same direction for elevator commands and in opposite directions for aileron commands.

The total build time for the vehicle was 11 hours and the final prototype is shown in Fig. 5.16. Table 5.16 shows the time devoted to each portion of the build process and

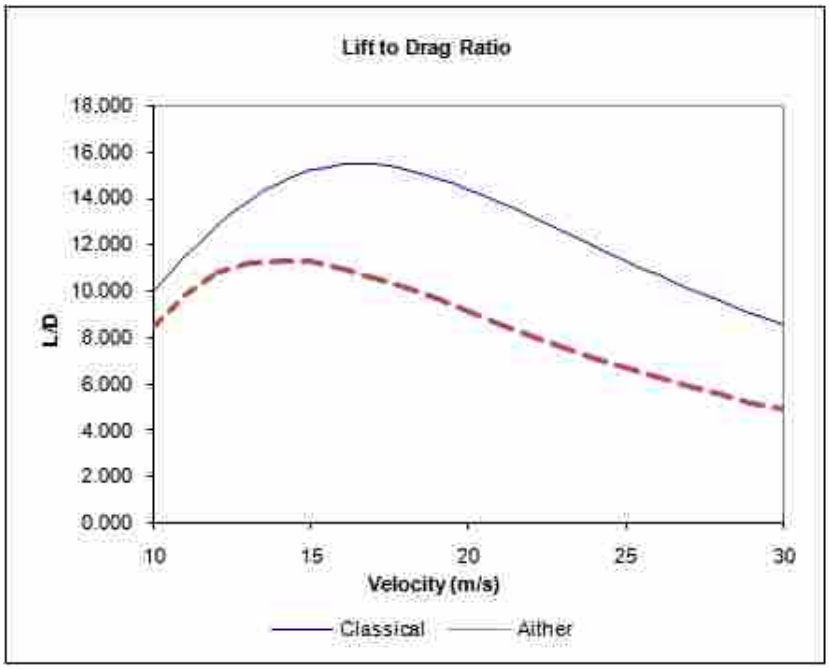

Figure 5.14: Lift to Drag Ratio

Table 5.16: Aircraft Build Time

Task	**Time (hr)**
Cut and assemble foam wing and body cores	3
Build and attach motor mount	1
Apply bi-directional fiber tape and colored tape	.5
Layup and vacuum bag propeller shroud	3
Build and attach winglets and elevons	.5
Attach motor and ESC	.5
Attach servos and radio receiver	1
Build and attach control vanes	1
Balance aircraft and attach battery	.5
Total	11

the order of construction. The actual mass of the vehicle including the 200 gram payload was 1374 grams. A comparison of the estimated mass of the aircraft with the actual mass is shown in Table 5.17. The structure weight fraction was .376 compared to the predicted value of .314. Table 5.17 shows that the most significant errors occurred in the fiber tape covering and the miscellaneous structure mass estimates.

Table 5.17: Aircraft Mass

Item	**Estimated Mass (g)**	**Actual Mass (g)**	**Error (g)**	**% Error**
Left Outboard Wing Core	24.9	22.3	-2.5	-.20%
Left Inboard Wing Core	10.3	9.8	-.5	.04%
Body Core	56.6	58.9	2.4	.19%
Right Inboard Wing Core	10.3	9.6	-.8	-.06%
Right Outboard Wing Core	24.9	23.0	-1.8	-.15%
Fiber Tape Covering	95.3	122.6	27.2	2.18%
Propeller Shroud	70	58.1	-11.9	-.95%
Miscellaneous Structure	100	213.0	113.1	9.05%
Motor and Propeller	220	241.0	21.0	1.68%
Electronic Speed Control	70	66.8	-3.2	-.26%
Servos	72	72.0	0.0	.00%
Radio Receiver	30	11.8	-18.2	-1.46%
Battery	265	265.0	0.0	.00%
Payload	200	200.0	0.0	.00%
Totals	1249	1374	124.8	9.99%

5.5.4 Flight Testing

Flight testing of the vehicle was carried out in two phases, vertical and horizontal. Horizontal flight testing was done outdoors while vertical flight testing was done with the vehicle tethered indoors. Battery voltage was recorded before and after each flight to get an average value. Flight time was recorded automatically by the radio transmitter, with the timer counting whenever the throttle setting was above 7%. Batteries were recharged after each flight and the total capacity needed to recharge each battery was recorded. The average current from the battery per flight was calculated by dividing the battery capacity used by the flight time. The average current was multipled by the average voltage to give the average power consumption of the aircraft in flight.

Three different tethered vertical flight tests were performed with the airplane. First, the aircraft was restrained to allow only vertical motion and flown to ensure adequate thrust for hovering and climbing vertically. These tests were done both without and with the 200 gram payload. In both cases, the aircraft was able to rise vertically, hover, and return to the landing position. The tests without the payload proved that the vehicle could hover for

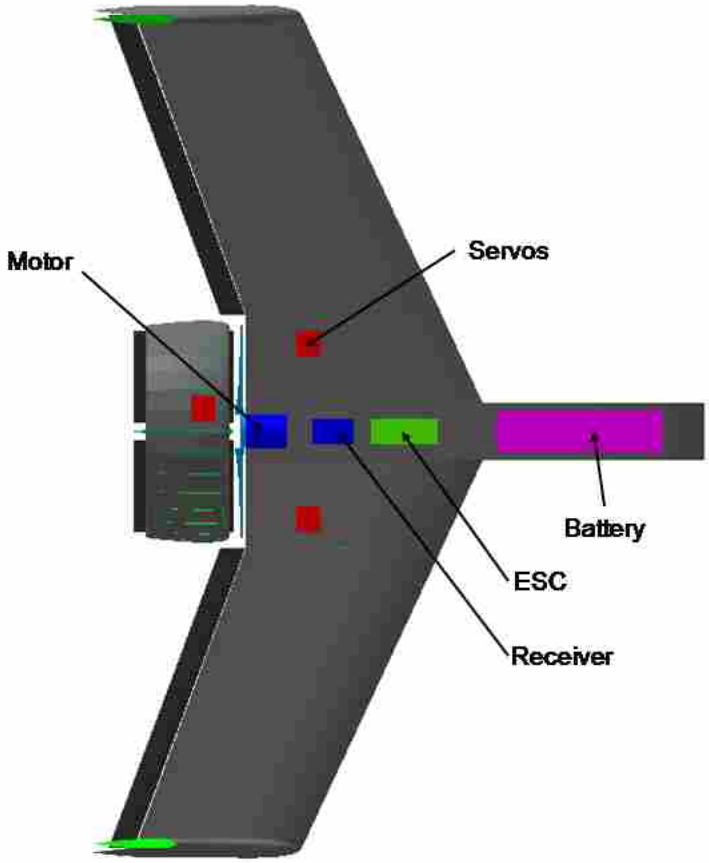

Figure 5.15: Component Placement

Figure 5.16: Final Prototype

Table 5.18: Prototype 4 Vertical Flight Testing

Flight	Propeller (inch)	Time (min:sec)	Capacity Used (mAh)	Voltage (V)	Current (A)	Power (W)
1	10x6	1:21	631	12.2	30.4	362
2	10x6	1:11	546	12.15	31.8	387
3	10x6	2:46	855	12.2	25	308
4	10x6	1:54	720	12.25	25	308
5	10x6	0:57	417	12.3	25	308

approximately two and a half minutes before the battery voltage dropped below the hover threshold. When the payload was added to the airframe, the total hover time was reduced to approximately one and a half minutes. Power consumption during both tests was around 340 watts with a current of 28 amps.

The next flight tests were performed with the aircraft tethered to the ceiling with a single rope and hanging just above the floor to check for controllability in ground effect. The throttle was advanced to a point where the thrust produced was just below the weight of the vehicle, and then the control in all three axes were tested. The aircraft responded very well to rudder and aileron inputs and was able to be stabilized quite easily. Response to elevator inputs was non-symmetric but still adequate to allow the vehicle to remain in control. The pitch response to up elevator control inputs was much faster and much more pronounced than the response to down elevator inputs. The test demonstrated that the control system was adequate to provide control in ground effect.

The final tethered vertical flight test was similar to the previous tests. The only difference between the two tests was the height of the aircraft above the floor. The height was increased to approximately two meters inorder to verify controllabiliy of the vehicle while in vertical flight out of ground effect. The results of the test were similar to the ground effect test. The control response in roll and yaw was excellent, while the control in pitch was adequate but non-symmetric. The test demonstrated that the vehicle had adequate control in vertical flight out of ground effect. Table 5.18 shows the results of all the vertical flight testing.

Table 5.19: Prototype 4 Horizontal Flight Testing

Flight	Propeller (inch)	Time (min:sec)	Capacity Used (mAh)	Voltage (V)	Current (A)	Power (W)
1	10x6	8:27	1954	12.15	13.9	169
2	10x6	3:03	740	12.25	14.6	178

Horizontal flight testing was done to verify predictions of power and stability, as with the previous prototypes. The tests showed that the stabilty of the aircraft was predicted effectively. The initial flight with this aircraft was difficult, as the aircraft flew with an excessively nose-up attitude. When the aircraft was trimmed, it flew well and was completely controllable. The aircraft performance during the trimming process was amazing, as it flew through several stalls and was easily recovered with no significant loss in altitude owing to the high thrust-to-weight ratio and the control afforded by the control vanes. Table 5.19 shows the data from the flight tests with the fourth prototype.

5.5.5 Prototype 4 Summary

Design, construction and flight testing of the fourth prototype incorporated all the lessons learned from the previous prototypes. The design was successfull and flew both vertically and horizontally. The flight tests with this prototype showed that the wings need additional reinforcement. During hard turns at speeds above 15 m/s, the outboard sections of the wing would flex. The aircraft was still controllable and flyable, but observation showed that reinforcement was necessary. This flexibility was not observed in the previous prototypes and was due to the higher aspect ratio of the outboard wing sections and the wing joint between the inboard and outboard sections. The predictions for power from Aither were more accurate than the classic design methods, but both methods underpredicted the power required and thus the total flight time was less than predicted as well for this and all prototypes.

Chapter 6

Conclusions and Recommendations

6.1 Conclusions

The flying wing concept proved to be a viable design option for a tail-sitter UAV. The original objective of the project was to design, build and fly the smallest useful VTOL tail-sitter UAV to date. This objective was achieved. The original anticipated challenges, control in descending vertical flight and development of a strong but light weight airframe, were overcome. Tables 6.1 and 6.2 show the desired and actual values for all of the design requirements and parameters. While not all of these requirements were met, the aircraft was successfully designed, built, and flown. The design process and the Aither analysis software proved to be useful tools in the development of the tail-sitter.

Table 6.1: Design Requirement Results

Desired Value	**Actual Value**
No exposed propeller	No exposed propeller
Horizontal flight by an average RC pilot Horizontal and vertical flight by autopilot	Flown horizontally by an average RC pilot Flown vertically while tethered and demonstrated adequate control
Build time of less than 10 hours	Build time 11 hours
5 hard landings without repair	3 hard landings without repair
Land vertically and conventionally	Lands conventionally and vertically

The most significant achievement with this aircraft was the development of a control system that was effective for vertical flight while the vehicle was descending or hovering in ground effect. The most challenging aspect of the project was developing a design solution that allowed the aircraft to achieve the desired flight time while hovering. As seen in

Table 6.2: Design Parameter Results

Design Parameter	**Desired Value**	**Actual Value**
Useful payload	.20 kilograms	.20 kilograms
Hover endurance	10 minutes	2.5 minutes
Loiter endurance	30 minutes	15 minutes
Ground footprint	.14 meter ^{2}	.24 meter ^{2}
Minimum Thrust-to-Weight ratio	1.3	1.28
Maximum Dimension	1 meter	1 meter
Maximum Mass	1.50 kilograms	1.37 kilograms
Cruise airspeed	15 m/s	15 m/s

Table 6.2, the total flight times in hover and vertical flight were less than the desired values. However, the aircraft was able to be built within the alloted size and weight limits and with an adequate thrust-to-weight ratio. In addition, the design of the aircraft was very safe. No propellers were damaged in any flight test and no damage was incurred by any of the components on the aircraft. The build time for the aircraft was 11 hours, which was slightly over the desired time, but still adequate to show that the airframe was simple and easy to build. The use of an electric propulsion system proved to be problematic for the tail-sitter because the maximum thrust decreased during flight due to the decrease in battery voltage.

6.2 Recommendations

Through the design and development of this aircraft, four specific recommendations drew my attention as possible areas of improvement on this design and on other tail-sitter design concepts. These were the use of counter-rotating propellers, vectored thrust, variable pitch propellers and improved propulsion technology.

Coaxial counter-rotating propellers have the possibility of greatly improving the performance of a tail-sitter. The counter-rotating arrangement would almost completely eliminate the torque produced by the propulsion system. On this aircraft, the control vanes placed in the propeller slipstream had to be slightly deflected at all times in order to counter the torque while the vehicle was hovering in a vertical attitude. This decreased the maximum thrust available from the propulsion system which in turn reduced the efficiency of the propulsion system, the thrust-to-weight ratio, and the total hover flight time. Currently,

there are at least two coaxial counter-rotating motor systems available commercially for small electric aircraft, but they were not in the acceptable power range for use on this aircraft.

Employing a thrust vectoring system on the tail-sitter UAV could eliminate the need for control vanes placed in the propeller slipstream. A 2-axis gimble design for the motor could allow thrust vectoring in two dimensions, controlling pitch and yaw while in vertical flight. In addition, if the thrust vectoring system was coupled with a coaxial counter-rotating propulsion system, roll control could be achieved by varying the rotational speed of each propeller independently. This method could allow complete control of the vehicle in all three axes without the employment of control vanes.

The use of variable pitch propellers would greatly improve the efficiency of the propulsion system by allowing the pitch of the propeller to be changed to match flight conditions. During low speed flight and hovering maneuvers, a propeller with low pitch is desirable, while in high speed forward flight a higher pitch becomes more advantageous. Thus, a variable pitch propeller system has the potential to improve efficiency, thrust-to-weight ratio, and flight times in both vertical and horizontal flight.

Improved propulsion technology will certainly make the future design and implementation of tail-sitter UAVs more prolific. Both better batteries and the use of gas propulsion systems could improve tail-sitter designs. The batteries used on this aircraft worked well, but flight times were less than expected because the battery drained quickly. Also, vertical flight became impossible after the battery voltage had dropped significantly, which negated the possibility of a vertical landing after a long flight. Batteries with a greater energy density could improve flight times without adding additional weight to the aircraft. Gas propulsion has great potential in a tail-sitter UAV for two reasons. First, the maximum thrust of the aircraft does not change during a flight as it does in an electrically powered vehicle. Second, the weight of the vehicle actually decreases during flight due to fuel burn. This means that the thrust-to-weight ratio would actually increase when using a gas propulsion system, which would allow vertical landing even after long flights.

References

[1] D. P. Raymer, *Aircraft Design: A Conceptual Approach*, 4th ed. 1801 Alexander Bell Drive, Reston, Virginia 20191-4344: American Institute of Aeronautics and Astronautics, 2006. 2, 4

[2] B. McCormick, *Aerodynamics of V/STOL Flight*. New York, New York 10003: Academic Press Inc., 1967. 2, 6, 25

[3] R. B. Stoney, "Design, Fabrication, and Test of a Vertical Attitude Takeoff and Landing Unmanned Air Vehicle," Master's thesis, Naval Postgraduate School, Monterey, CA, 1993. 4

[4] W. A. Newsome and J. R. Anglin, "Free-Flight Model Investigation of a Vertical-Attitude VTOL Fighter," NASA, Hampton, Virginia, Technical Note TN D-8054, 1975. 6

[5] Hobby Lobby International Inc., http://www.hobby-lobby.com/. 7, 27

[6] N. B. Knoebel, "Adaptive Quaternion Control of a Miniature Tailsitter UAV," Master's thesis, Brigham Young University, Provo, Utah, 2007. 7

[7] K. T. Ulrich and S. D. Eppinger, *Product Design and Development*, 3rd ed. 1221 Avenue of Americas, New York, NY 10020: McGraw-Hill/Irwin, 2004. 11

[8] R. H. Stone, "The T-wing tail-sitter unmanned air vehicle: from design concept to research flight vehicle," *Journal of Aerospace Engineering*, vol. 218, pp. 417–433, 2006. 14

[9] K. G. Wernicke, "The Single-Propeller Driven Tailsitter is the Simplest and Most Efficient Configuration for VTOL UAVs," *2000 International Powered Lift Conference Proceedings*, vol. 1, 2000. 14

[10] T. C. Corke, *Design of Aircraft*. Upper Saddle River, N.J.: Prentice Hall, 2003. 19

[11] W. J. Bowman and D. O. Snyder, "AIAA 2005-282 A Minimalist Approach to Teaching Aircraft Design." 43rd AIAA Aerospace Sciences Meeting and Exhibit, 2005. 19

[12] M. Drela, "XFOIL Subsonic Airfoil Development System," 2008, http://web.mit.edu/drela/Public/web/xfoil/. 20

[13] J. D. Anderson, *Aircraft Performance and Design*. Singapore: WCB McGraww-Hill, 1999. 20, 22, 24

[14] ——, *Fundamentals of Aerodynamics*, 3rd ed. 1221 Avenue of the Americas, New York, NY 10020: McGraw-Hill, 2001. 21, 57

[15] W. J. Phillips, *Mechanics of Flight*, 1st ed. 111 River Street, Hoboken, NJ 07030: John Wiley and Sons, 2006. 25, 37, 39, 40

[16] J. Seddon and S. Newman, *Basic Helicopter Aerodynamics*, 2nd ed. 1801 Alexander Bell Drive, Reston, VA 20191: American Institute of Aeronautics and Astronautics, Inc., 2001. 25

[17] D. F. Hunsaker, "A Numerical Vortex approach to Aerodynamic Modeling of SUAV/VTOL Aircraft," Master's thesis, Brigham Young University, Provo, Utah, 2006. 33

[18] J. Roskam, *Airplane Flight Dynamics and Automatic Flight Controls*. 120 East Ninth Street, Suite 2, Lawrence, KS66044: DARcorporation, 2001, vol. 1. 37, 40

[19] F. Wergeland, "The Great Electric Motor Test," 2004, www.flyingmodels.org. 58

[20] N. B. Knoebel, S. R. Osborne, D. O. Snyder, T. W. McLain, R. W. Beard, and A. M. Eldredge, "AIAA 2006-6713 Preliminary Modeling, Control, and Trajectory Design for Miniature Autonomous Tailsitters." Keystone, Colorado: AIAA Guidance, Navigation, and Control Conference and Exhibit, 21 - 24 August 2006. 63

[21] F. Fanelli, *R/C Ducted Fans*. P.O. Box 2, 729 Prospect Avenue, Osceola, WA 54020: Motorbooks International Publishers and Wholesalers Inc., 1987.

[22] R. W. Fox, A. T. McDonald, and P. J. Prichard, *Introduction to Fluid Mechanics*, 6th ed. 111 River Street, Hoboken, NJ 07030: John Wiley and Sons, 2004.

[23] D. James, *Ducted Fans for Model Jets*. Argus House, Boundary Way, Hemel Hempstead, Hertfordshire HP2 7ST, England: Argus Books, 1989.

[24] B. R. Munson, D. F. Young, and T. H. Okiishi, *Fundamentals of Fluid Mechanics*, 5th ed. 111 River Street, Hoboken, NJ 07030: John Wiley and Sons, 2006.

[25] L. R. Newcome, *Unmanned Aviation: A Brief History of Unmanned Aerial Vehicles*. Reston, Virginia: American Institute of Aeronautics and Astronautics, 2004.

[26] M. Simons, *Model Aircraft Aerodynamics*, 4th ed. P.O. Box 327 Poole Dorset BH15 2RG: Special Interest Model Books, 1999.

Appendix A

Wing Properties Program

The source code for the Wing Properties program is contained in this appendix. The program uses the root and tip airfoil points, root and tip chords, wing section semi-span, and leading edge sweep to calculate the volume and center of mass of a linearly swept and linearly tapered wing section with constant density. The input to the program is a text file with the following format:

rootAirfoil: naca0015.txt
tipAirfoil: naca0015.txt
rootChord: .4
tipChord: .20
span: 1.
LEsweep(deg): 45
density: 1.
sections: 50000

The output of the program first lists the areas and the centroids of the root and tip airfoils. Then the wing center of mass, total volume, and total mass are listed

```
/*
  Name: Wing Analysis program
  Copyright: 2007 Jeff Hogge
  Author: Jeff Hogge
  Date: 09/10/07 16:18
  Description: calculate the volume and centroid of a linearly tapered and
swept wing
*/

#include <vector>
#include <string>
#include <iostream>
#include <fstream>
#include <cmath>

using std::cout;
using std::endl;
using std::string;
using std::vector;
using std::ifstream;
using std::ofstream;
using std::ostream;

//Point class declaration
class Point
{
public:
    Point();
    Point(const Point &init);
    Point(double x, double y, double z);
    Point(double x, double y);
    ~Point(){};
    //operators
    Point & operator=(const Point &rhs);
    Point & operator+=(const Point &rhs);
    Point & operator-=(const Point &rhs);
    Point operator+(const Point &rhs);
    Point operator-(const Point &rhs);
    bool operator==(const Point &other) const;
    bool operator!=(const Point &other) const;
    // get functions
    double mag();
    double x();
    double y();
    double z();
    //set functions
    void setX(double val);
    void setY(double val);
    void setZ(double val);

    friend ostream& operator<<(ostream& os, Point& A);

private:
    double mPoint[3];
};

// ostream operator
```

```
ostream& operator<<(ostream& os, Point& A);

//cross product
Point cross(Point A, Point B);

////////////// main program
int main(void)
{
    //read in input file info
    ifstream in("wing_input.txt");
    //ensure input file is found
    if(!in.good())
    {
        cout<<"Error: input file not found."<<endl;
        system("pause");
        return 0;
    }
    //define variables to be used
    double rootXc, rootYc, rootArea, tipXc, tipYc, tipArea, volume, wingXc,
wingYc;
    int sections = 50000;

    //read in the data in the input file
    string dummy, rootFile, tipFile;
    double root, tip, span, sweep, density;
    in>>dummy;// <- this is a label in the input file
    in>>rootFile;
    in>>dummy;
    in>>tipFile;
    in>>dummy;
    in>>root;
    in>>dummy;
    in>>tip;
    in>>dummy;
    in>>span;
    in>>dummy;
    in>>sweep;//<- leading edge sweep
    in>>dummy;
    in>>density;
    in>>dummy;
    in>>sections;

    //echo the input data
    cout<<"\nRoot File:\t"<<rootFile<<endl;
    cout<<"Tip File:\t"<<tipFile<<endl;
    cout<<"Root chord:\t"<<root<<endl;
    cout<<"Tip chord:\t"<<tip<<endl;
    cout<<"Span:\t\t"<<span<<endl;
    cout<<"Sweep:\t\t"<<sweep<<endl;
    cout<<"Density:\t\t"<<density<<endl;
    cout<<"Sections:\t"<<sections<<endl;

    //convert sweep to radians
    sweep = sweep * 3.14159265359/180.;

    //close the input file
    in.close();
```

```
//open the root file and read in the data
ifstream rootin(rootFile.c_str());
if(!rootin.good())
{
    cout<<"Error: Problem with root airfoil file."<<endl;
    return 0;
}
//read in the airfoil name from the first line
getline(rootin,dummy);

//create a vector of points
vector<Point*> point;

//read in the root airfoil data
int n = 0;
while(!rootin.eof())
{
    double x,y;
    rootin>>x;
    rootin>>y;
    Point *pt = new Point;
    pt->setX(x);
    pt->setY(y);
    point.push_back(pt);
    n++;
}
//close the root airfoil file
rootin.close();

//calculate the area
Point A = *point[1];
Point B = *point[0];
Point C = *point[n-2];

int swap = 1, ct = 0;
double Area = 0., Xc = 0., Yc = 0.;
while(ct < n/2)
{
    //define two vectors that border the triangle
    Point x1 = A-B;
    Point x2 = C-B;
    //calculate the area of the triangle and add to the running total
    double a =.5*cross(x1,x2).mag();
    Area += a;
    //find the location of the triangle centroid
    double m1 = (A.y()+B.y()-2.*C.y())/(A.x()+B.x()-2.*C.x());
    double m2 = (2.*A.y()-B.y()-C.y())/(2.*A.x()-B.x()-C.x());
    double xc = (A.y()-m2*A.x()-C.y()+m1*C.x())/(m1-m2);
    double yc = (m1*m2*(A.x()-C.x())+C.y()*m2-A.y()*m1)/(m2-m1);
    //zero the triangles that have negligible area
    if(a < 1e-12)
    {
        a = 0.;
        xc = 0.;
        yc = 0.;
    }
```

```
        Yc += yc*a;
        Xc += xc*a;
        //update the points to use in finding vectors x1 and x2
        B = C;
        C = A;
        //alternate the triangles between upper and lower
        if(swap)
        {
            A = *point[n-ct-2];
            swap = 0;
        }
        else
        {
            A = *point[ct+1];
            swap = 1;
        }
        ct++;
    }
    //calculate the centroid
    rootXc = Xc/Area*root;
    rootYc = Yc/Area*root;
    rootArea = Area*root*root;
    cout<<"\nRoot airfoil centroid: "<<rootXc<<" , "<<rootYc<<endl;
    //show the root airfoil area
    cout<<"Root airfoil area:\t"<<rootArea<<endl;

    //check to see if root and tip are the same airfoil
    if(rootFile == tipFile)
    {
        tipXc = Xc/Area*tip;
        tipYc = Yc/Area*tip;
        tipArea = Area*tip*tip;
        cout<<"\nTip airfoil centroid: "<<tipXc<<" , "<<tipYc<<endl;
        //show the root airfoil area
        cout<<"Tip airfoil area:\t"<<tipArea<<endl;
    }
    else
    {
        //repeat calculations for the tip
        //open the tip file
        ifstream tipin(tipFile.c_str());
        if(!tipin.good())
        {
            cout<<"Error: Problem with tip airfoil file."<<endl;
            return 0;
        }
        //read in the airfoil name from the first line
        getline(tipin,dummy);
        cout<<dummy<<endl;
        //clear the points vector
        point.clear();
        //read in the tip airfoil data
        n = 0;
        while(!tipin.eof())
        {
            double x,y;
            tipin>>x;
```

```
    tipin>>y;
    Point *pt = new Point;
    pt->setX(x);
    pt->setY(y);
    point.push_back(pt);
    n++;
}
//close the tip airfoil file
tipin.close();

//reset variables
swap = 1, ct = 0;
Area = 0., Xc = 0., Yc = 0.;
//calculate the area
A = *point[1];
B = *point[0];
C = *point[n-2];
while(ct < n/2)
{
    //define two vectors that border the triangle
    Point x1 = A-B;
    Point x2 = C-B;
    //calculate the area of the triangle and add to the running total
    double a =.5*cross(x1,x2).mag();
    Area += a;
    //find the location of the triangles centroid
    double m1 = (A.y()+B.y()-2.*C.y())/(A.x()+B.x()-2.*C.x());
    double m2 = (2.*A.y()-B.y()-C.y())/(2.*A.x()-B.x()-C.x());
    double xc = (A.y()-m2*A.x()-C.y()+m1*C.x())/(m1-m2);
    double yc = (m1*m2*(A.x()-C.x())+C.y()*m2-A.y()*m1)/(m2-m1);
    //zero the triangles that have negligible area
    if(a < 1e-10)
    {
        a = 0.;
        xc = 0.;
        yc = 0.;
    }
    Yc += yc*a;
    Xc += xc*a;
    //update the points to use in finding vectors x1 and x2
    B = C;
    C = A;
    //alternate the triangles between upper and lower
    if(swap)
    {
        A = *point[n-ct-2];
        swap = 0;
    }
    else
    {
        A = *point[ct+1];
        swap = 1;
    }
    ct++;
}
tipXc = Xc/Area*tip;
tipYc = Yc/Area*tip;
```

```
        tipArea = Area*tip*tip;
        cout<<"\nTip airfoil centroid: "<<tipXc<<" , "<<tipYc<<endl;
        //show the root airfoil area
        cout<<"Tip airfoil area:\t"<<tipArea<<endl;
    }

    //calculate wing volume and centroid with sections
    volume = 0.;
    wingXc = 0.;
    wingYc = 0.;
    double delx = span/double(sections);
    for(int i = 0; i <= sections; i++)
    {
        double f = delx*double(i)/span;
        double ai =(1.-f)*rootArea+f*tipArea;
        double yc = (1.-f)*rootXc+f*tipXc;
        //volume
        volume += ai*delx;
        //x centroid
        wingXc +=ai*delx*(double(i)*delx + delx/2.);
        //y centroid
        wingYc += ai*delx*(double(i)*delx*tan(sweep) + yc);
    }
    wingXc = wingXc/volume;
    wingYc = wingYc/volume;
    cout<<"\nWing centroid:\t"<<wingXc<<" , "<<wingYc<<endl;
    cout<<"Wing Volume:\t"<<volume<<endl;
    cout<<"Wing Mass:\t"<<density*volume<<endl;

    system("pause");
    return 0;
}

////////////////////  Point class implementation
Point::Point()
{
    mPoint[0] = 0.;
    mPoint[1] = 0.;
    mPoint[2] = 0.;
}

Point::Point(const Point &init)
{
    *this = init;
}

Point::Point(double x, double y, double z)
{
    mPoint[0] = x;
    mPoint[1] = y;
    mPoint[2] = z;
}

Point::Point(double x, double y)
{
    mPoint[0] = x;
    mPoint[1] = y;
```

```
    mPoint[2] = 0.;
}

//operators
Point& Point::operator=(const Point &rhs)
{
    //check for self assignment
    if(this == &rhs) return *this;
    mPoint[0] = rhs.mPoint[0];
    mPoint[1] = rhs.mPoint[1];
    mPoint[2] = rhs.mPoint[2];
    return *this;
}

Point& Point::operator+=(const Point &rhs)
{
    mPoint[0] += rhs.mPoint[0];
    mPoint[1] += rhs.mPoint[1];
    mPoint[2] += rhs.mPoint[2];
    return *this;
}

Point& Point::operator-=(const Point &rhs)
{
    mPoint[0] -= rhs.mPoint[0];
    mPoint[1] -= rhs.mPoint[1];
    mPoint[2] -= rhs.mPoint[2];
    return *this;
}

Point Point::operator+(const Point &rhs)
{
    Point sum(*this);
    sum += rhs;
    return sum;
}

Point Point::operator-(const Point &rhs)
{
    Point diff = *this;
    diff -= rhs;
    return diff;
}

bool Point::operator==(const Point &other) const
{
    if(mPoint[0] == other.mPoint[0] && mPoint[1] == other.mPoint[1] &&
mPoint[2] == other.mPoint[2])
    {
        return true;
    }
    else return false;
}

bool Point::operator!=(const Point &other) const
{
    return !(*this == other);
```

```
}

// get functions
double Point::mag()
{
    return sqrt( mPoint[0]*mPoint[0] + mPoint[1]*mPoint[1] +
mPoint[2]*mPoint[2]);
}

double Point::x()
{
    return mPoint[0];
}

double Point::y()
{
    return mPoint[1];
}

double Point::z()
{
    return mPoint[2];
}

//set functions
void Point::setX(double val)
{
    mPoint[0] = val;
    return;
}

void Point::setY(double val)
{
    mPoint[1] = val;
    return;
}

void Point::setZ(double val)
{
    mPoint[2] = val;
    return;
}
//point ostream operator
ostream& operator<<(ostream& os, Point& A)
{
    os<<A.x()<<" , "<<A.y()<<" , "<<A.z();
    return os;
}
//cross product operator
Point cross(Point A, Point B)
{
    Point result;
    result.setX(A.y()*B.z() - A.z()*B.y());
    result.setY(-1.*(A.x()*B.z() - A.z()*B.x()));
    result.setZ(A.x()*B.y() - A.y()*B.x());
    return result;
}
```